Crosstalk between H2A variant-specific modifications impacts vital cell functions

Anna Schmücker[1¶], Bingkun Lei[1¶], Zdravko J. Lorković[1], Matías Capella[2], Sigurd Braun[2,3] Pierre Bourguet[1,4], Olivier Mathieu[4], Karl Mechtler[1], and Frédéric Berger[1*]

[1] Gregor Mendel Institute (GMI), Austrian Academy of Sciences, Vienna BioCenter (VBC), Dr. Bohr-Gasse 3, 1030 Vienna, Austria.

[2] Biomedical Center, Department of Physiological Chemistry, Ludwig-Maximilians-University of Munich, Großhaderner Straße 9, 82152 Planegg-Martinsried, Germany

[3] International Max Planck Research School for Molecular and Cellular Life Sciences, Am Klopferspitz 18, 82152 Planegg-Martinsried, Germany

[4] CNRS, Université Clermont Auvergne, Inserm, Génétique Reproduction et Développement (GReD), F-63000 Clermont-Ferrand, France

[*]Corresponding author:
Email: Frederic.berger@gmi.oeaw.ac.at (FB)

¶ These authors contributed equally to this work.

Gregor Mendel Institute of Molecular Plant Biology

Dr. Bohr-Gasse 3

1030 Vienna, Austria

Tel: +43-1-79044-9810

E-mail: frederic.berger@gmi.oeaw.ac.at

Abstract

Histone variants are distinguished by specific substitutions and motifs that might be subject to post-translational modifications (PTMs). Compared with the high conservation of H3 variants, the N- and C-terminal tails of H2A variants are more divergent and are potential substrates for a more complex array of PTMs, which have remained largely unexplored. We used mass spectrometry to inventory the PTMs of the two heterochromatin-enriched variants H2A.W.6 and H2A.W.7 of *Arabidopsis*, which harbor the C-terminal motif KSPK. This motif is also found in macroH2A variants in animals and confers specific properties to the nucleosome. We showed that H2A.W.6 is phosphorylated by the cell cycle-dependent kinase CDKA specifically at KSPK. In contrast, this modification is absent on H2A.W.7, which also harbors the SQ motif associated with the variant H2A.X. Phosphorylation of the SQ motif is critical for the DNA damage response but is suppressed in H2A.W.7 by phosphorylation of KSPK. To identify factors involved in this suppression mechanism, we performed a synthetic screen in fission yeast expressing a mimic of the *Arabidopsis* H2A.W.7. Among those factors was the BRCT-domain protein Mdb1. We showed that phosphorylation of KSPK prevents binding of the BRCT-domain protein Mdb1 to phosphorylated SQ and as a result hampers response to DNA damage. Hence, cross-talks between motif-specific PTMs interfere with the vital functions of H2A variants. Such interference could be responsible for the mutual exclusion of specific motifs between distinct H2A variants. We conclude that sequence innovations in H2A variants have potentiated the acquisition of many specific PTMs with still unknown functions. These add a layer of complexity to the nucleosome properties and their impact in chromatin regulation.

Introduction

Histones represent the major protein component of chromatin. Histone variants evolved in all core histone families and acquired comparable properties in a convergent manner [1-4]. These variants play major roles in cell fate decisions, development, and disease [5-7]. Most

58 multicellular eukaryotes contain three types of H2A variants: H2A, H2A.Z and H2A.X. The
59 variant H2A.X is defined by the motif SQ[E/D]Φ present within the C-terminal tail (where Φ
60 stands for a hydrophobic amino acid) that is present only at the C-terminal tail of H2A.X. The
61 serine residue of this motif is phosphorylated during the early phase of the DNA damage
62 response (DDR) [7-11]. In animals, serine 139 (S139) phosphorylation at the SQ motif of
63 H2A.X (γH2A.X) is sufficient to recruit the mediator of DNA damage checkpoint protein 1
64 (MDC1) [12]. In contrast, MDC1 binding is abolished if tyrosine 142 (Y142) of γH2A.X is
65 phosphorylated. Thus, the succession of these two phosphorylation steps dictates the order of
66 events at sites of DNA damage [13-15]. In plants and yeast, serine phosphorylation of
67 SQ[E/D]Φ is also essential for DDR although Y142 of H2A.X is not conserved [16, 17]. At the
68 initiation of DDR in fission yeast, γH2A.X is recognized by the BRAC1 C-terminal (BRCT)
69 domains of Crb2 [18] and Mdb1, the ortholog of human MDC1 [19]. These events are
70 genetically redundant and initiate formation of radiation-induced nuclear foci at the site of DNA
71 damage, which act as template for recruiting DNA repair machinery. BRCT domain-containing
72 proteins also exist in plants, yet their functions remain unknown.

73 In *Arabidopsis*, in addition to H2A.X, DDR also relies on the plant specific variant
74 H2A.W.7 that harbors an SQ motif at the C-terminal tail [9, 16, 20]. The family of H2A.W
75 variants evolved in land plants, where they exclusively occupy constitutive heterochromatin,
76 and consists of three isoforms in *Arabidopsis* (H2A.W.7, W.6 and W.12) [2, 16, 21]. H2A.W
77 confers distinct properties to the nucleosome through differences in its primary amino acid
78 sequence in the L1 loop, the docking domain, and the extended C-terminal tail [22]. The main
79 feature defining H2A.W variants is the C-terminal KSPK motif [21, 23]. Due to the expected
80 location of the H2A.W C-terminus at the nucleosome dyad (entry/exit site of the DNA into the
81 nucleosome), the KSPK motif is placed in a functionally significant area [24] where it interacts
82 with the linker DNA [25]. This motif is a member of the S/T-P-X-K/R motifs (where X
83 represents any amino acid) present in macroH2A in metazoans and linker histones H1 among

84 other proteins [26-32]. Both H2A.W and macroH2A are required for heterochromatin
85 organization, suggesting a potential convergence in the function of these histone variants [2].
86 Incorporation of these variants confers specific biophysical properties to the nucleosomes and
87 chromatin [1, 26, 33, 34].

88 Distinct C-terminal motifs present in specific classes of H2A variants do not usually co-
89 occur. The KSPK is present exclusively in plant H2A.W and mammalian macroH2A, while the
90 SQ[E/D]Φ motif is present primarily on H2A.X variants in eukaryotes [5, 9, 33, 35]. There are
91 notable exceptions to this rule in animals and plants. *Drosophila* H2A.V combines the
92 SQ[E/D]Φ motif with properties of H2A.Z [36]. Several species of seed-bearing plants possess
93 a subtype of H2A.W that also harbors a SQ[E/D]Φ motif [16]. In *Arabidopsis*, H2A.X is largely
94 excluded from constitutive heterochromatin, which is occupied by the variant H2A.W.7 that
95 carries both the SQ[E/D]Φ and KSPK motifs. H2A.X and H2A.W.7 are essential to mediate
96 the response to DNA damage in *Arabidopsis*, but variants similar to H2A.W.7 are present only
97 in a restricted number of flowering plant species [16]. What led to the mutual exclusion of C-
98 terminal motifs during H2A variant evolution has remained unclear, but one reason could be
99 incompatibility between post-translational modifications (PTMs) on variant specific motifs.

100 Different types and combinations of PTMs of core histones coordinate the recruitment
101 of proteins that dictate chromatin configuration and consequently regulate genome integrity and
102 genome expression [5, 7, 15, 37-39]. Non-centromeric H3 variants share strong sequence
103 homology and, with a few exceptions [40-42], are subjected to the same repertoire of
104 modifications. In contrast, sequence homology between H2A variants, particularly at their N-
105 and C-terminal tails, is much less pronounced [23, 33]. This provides opportunities for
106 deposition of distinct patterns of modifications for each type of H2A variant [7, 43].

107 Here, we provide an inventory of PTMs of H2A.W variants in *Arabidopsis*, including
108 some that are specific of subtypes of H2A.W variants. H2A.W.6 is phosphorylated at the serine
109 residue of the KSPK motif, and we provide evidence that the modification is deposited by cyclin

110 dependent kinases (CDKs). In contrast, H2A.W.7 is only phosphorylated on the SQ motif.
111 Notably, H2A.W.7 carrying a phosphomimetic KDPK motif shows impaired DDR. Through a
112 synthetic approach in fission yeast, we show that phosphorylation of the KSPK motif prevents
113 Mdb1 binding to the phosphorylated SQ motif and proper DDR, suggesting that the absence of
114 KSPK phosphorylation in H2A.W.7 is essential for the SQ motif to mediate DDR in
115 *Arabidopsis*. Hence, PTMs of C-terminal motifs of the H2A.W.7 variant interfere with each
116 other and, during DDR this seems to be resolved by suppression of PTMs on the KSPK motif.
117 Yet, this type of variant remains rarely present in eukaryotes. We propose that incompatibility
118 between the PTMs carried by H2A variant specific motifs provide a possible explanation for
119 the mutual exclusion of C-terminal motifs between H2A variants.

120 **Results**

121 **H2A.W.6 and H2A.W.7 display distinct patterns of modifications at their C-terminal tails**

122 We immunopurified mononucleosomes containing H2A.W.6 or H2A.W.7 from wild type (WT)
123 leaves of *Arabidopsis* (Fig 1A and 1B) and performed qualitative MS analysis to identify PTMs
124 associated with each isoform. In both isoforms, N- and C-terminal tails were modified at several
125 lysine residues by acetylation and/or methylation (Fig 1C). A more complex set of
126 modifications was found on the C-terminal tail of H2A.W.6, with prevalence of lysine
127 acetylation and serine phosphorylation (Fig 1C). Although H2A.W.6 and H2A.W.7 exist
128 primarily as homotypic (two copies of either H2A.W.6 or H2A.W.7), heterotypic (one copy of
129 each H2A.W.6 and H2A.W.7) nucleosomes can be identified [16, 22] (Fig 1B). Importantly,
130 H2A.W.6 and H2A.W.7 precipitated in respective and reciprocal immunoprecipitations
131 contained similar sets of modifications (S1 Fig), suggesting that each variant isoform acquires
132 distinct modification patterns independently of the nucleosome composition. Some of these
133 modifications were specific to each isoform, in part due to the absence of conservation of the
134 residues targeted by these modifications. Three lysine residues at the N-terminal tails of

135 H2A.W.6 and H2A.W.7 present in a highly conserved sequence context (KSVSKSMKAG vs.
136 KSVSKSVKAG) showed similar PTMs in both variants. In contrast, other lysine residues at
137 the N-termini in a less conserved context displayed isoform-specific modifications (Fig 1C).
138 On both variants, acetylation was detected on lysine residue 128 and 144, which are embedded
139 in the same sequence context (Fig 1C). Seedlings, leaves and flowers showed similar patterns
140 of lysine modifications at the C-terminal tail, but they differed in their range and abundance.
141 The three serine residues (S129, S141, and S145) at the C-terminal tail were phosphorylated on
142 H2A.W.6 in leaves, as previously reported [44]. Based on spectral counting, the most abundant
143 phosphorylation was S145, followed by S141 and S129; the last one being very rare.
144 Phosphorylation of S141 and S145 were also detected on H2A.W.6 from seedlings, where a
145 single spectrum also detected S129 phosphorylation of H2A.W.7. In flowers, only S145 was
146 detected on H2A.W.6 (S1 Fig). Overall, the repertoire of PTMs detected on H2A.W.6 and
147 H2A.W.7 differed markedly (Fig 1C). As S145 of the conserved KSPK motif is part of the
148 functionally relevant C-terminal tail that protects the linker DNA [22, 23], we focused our
149 further analysis on S145 phosphorylation. We obtained an antibody that specifically binds
150 phosphorylated S145 in both H2A.W.6 and H2A.W.7 *in vitro* (S2 Fig). Yet, consistent with the
151 MS data, *in vivo* KSPK phosphorylation was only detected on H2A.W.6 (Fig 1C and 1D) and
152 we therefore named this antibody H2A.W.6p. Our data suggest that phosphorylation of the
153 KSPK motif is deposited on H2A.W.6 but not on H2A.W.7, which can be phosphorylated on
154 its SQ motif in response to DNA damage.

155 **The KSPK motif of H2A.W.7 is not phosphorylated upon DNA damage induction**

156 We investigated the modification of KSPK and SQ motifs in H2A.W.6, H2A.W.7, and H2A.X
157 after inducing DNA damage with bleomycin treatment. In WT, bleomycin treatment induced
158 phosphorylation of H2A.X and H2A.W.7 at the SQ motifs (γH2A.X and γH2A.W.7), as
159 previously reported [16] (Fig 2A). To determine whether bleomycin treatment induced
160 phosphorylation of KSPK on H2A.W.7, we applied two-hour treatment with bleomycin to *hta6*

161 mutant seedlings, which are deprived of H2A.W.6 and only expressed H2A.W.7 (Fig 2A).
162 Under these conditions, KSPK phosphorylation was not detected, suggesting that DDR does
163 not induce phosphorylation of KSPK on H2A.W.7. In conclusion, DNA damage triggers
164 phosphorylation of the SQ motif of H2A.X and H2A.W.7, but not of the KSPK motif of
165 H2A.W.7.

166 **H2A.W.6 phosphorylation is mediated by CDKA and is cell cycle dependent**

167 We observed that prolonged exposure to bleomycin caused a marked decrease of KSPK
168 phosphorylation of H2A.W.6 (Fig 2B). As DNA damage causes cell cycle arrest [45, 46], we
169 hypothesized that KSPK phosphorylation could be associated with cell cycle progression.
170 Because our *Arabidopsis* cell suspension could not be synchronized, we used tobacco BY-2 cell
171 suspension for cell cycle synchronization to address this question. In tobacco, six of the seven
172 H2A.W isoforms contain the KSPK motif at the C-terminus, of which phosphorylation was
173 detected by the H2A.W.6p antibody (S3A and S3B Fig). We analyzed H2A.W phosphorylation
174 status in synchronized tobacco BY-2 cells over a twelve-hour time course after release from an
175 aphidicolin-induced cell cycle block (S3C and S3D Fig). While H2A.W.6 levels were
176 comparatively stable throughout the cell cycle, phosphorylation of KSPK remained stable
177 during S and G2 but decreased during G1 phase (Fig 3A and S3E Fig). We tested whether levels
178 of H2A.W.6p also fluctuated in dividing cells of *Arabidopsis* root tips where pairs of small flat
179 cells in G1 are easily distinguished from larger cells in G2 phase (Fig 3B). Cells in S phase
180 were marked by a pulse of EdU incorporation. Consistent with results obtained with
181 synchronized BY-2 cells, *Arabidopsis* root tip nuclei in S, M, and G2 phases showed high levels
182 of H2A.W.6 phosphorylation, whereas this mark was not detected in G1 phase nuclei (Fig 3B).
183 This fluctuation was not the result of changes in total levels of H2A.W.6, which remained
184 relatively uniform throughout the cell cycle (S4A Fig). These results showed that
185 phosphorylation of H2A.W.6 is dependent on cell cycle progression.

186 We next tested the impact of cell cycle inhibition on H2A.W.6p levels. S phase arrest
187 by treatment with hydroxyurea or aphidicolin did not affect H2A.W.6 phosphorylation in
188 *Arabidopsis* cell suspension cultures (Fig 3C). In contrast, when we inhibited cyclin-dependent
189 kinases (CDKs) with roscovitine [47], H2A.W.6p was almost undetectable (Fig 3C). The
190 specificity and concentration dependence of H2A.W.6p inhibition by roscovitine (Fig 3C, S4B
191 Fig) prompted us to examine the *Arabidopsis* cyclin-dependent kinase CDKA;1, which is
192 predominantly active at the G1 to S-phase transition [48-50]. We immunopurified CDKA;1-
193 YFP from *Arabidopsis* seedlings and performed an *in vitro* kinase assay with recombinant
194 H2A.W.6-H2B, H2A.W.7-H2B, and H2A-H2B dimers (Fig 3D). We observed strong
195 phosphorylation of the H2A.W.6-H2B and H2A.W.7-H2B dimers but no signal in the H2A-
196 H2B control (Fig 3D), demonstrating that CDKA;1 phosphorylates H2A.W.6 and H2A.W.7 *in*
197 *vitro*. In plants with reduced CDKA;1 kinase activity [51, 52], we detected very low levels of
198 H2A.W.6 phosphorylation (S4C Fig), further supporting that CDKA;1 is the main kinase
199 responsible for H2A.W.6 modification. In root tips of plants with reduced CDKA;1 kinase
200 activity, only late G2/M-phase nuclei showed KSPK phosphorylation (S4D Fig). This
201 suggested that another CDK phosphorylates the KSPK motif in the absence of CDKA;1, which
202 might be CDKB;1, as it is active at the G2/M transition [49, 50, 53].
203 In conclusion, H2AW.6 is phosphorylated by cyclin-dependent kinases during the S,
204 G2, and M phases and the modification is likely removed during the G1 phase of the cell cycle.
205 **Cross talk between phosphorylation at the KSPK and SQ motifs in H2A.W.7**
206 We demonstrated that CDKA;1 phosphorylates H2A.W.7 at the KSPK motif *in vitro* (Fig 3D);
207 however, this modification was not detected *in planta* (Fig 1C and 1D, S2 Fig). We thus tested
208 whether DNA damage induced phosphorylation of the SQ motif interferes with KSPK
209 phosphorylation in H2A.W.7. This was not the case in *hta7* plants expressing phosphomimetic
210 (SQ to DQ) mutant forms of H2A.W.7 [16]. Additionally, KSPK phosphorylation was also not
211 observed when SQ phosphorylation was prevented in *hta7* plants expressing non-

212 phosphorylatable (SQ to AQ) (S5A Fig). Hence, phosphorylation of the H2A.W.7 SQ motif
213 does not appear to interfere with KSPK phosphorylation.

214 To test the crosstalk between SQ and KSPK phosphorylation *in planta*, we attempted to
215 complement the *hta7* mutant by expressing WT and mutant forms of H2A.W.7 (Fig 4A).
216 Expression of a mutant form of H2A.W.7 combining the WT SQ motif with a KDPK motif that
217 mimics phosphorylation (SQ-DP) did not rescue sensitivity of *hta7* mutant plants towards DNA
218 damage (Fig 4B). By contrast, mutation of the KSPK motif into non-phosphorylable KAPK
219 (SQ-AP) rescued DDR (Fig 4B). Notably, mutations of the KSPK motif into either KAPK or
220 KDPK did not affect SQ motif phosphorylation (Fig 4C). Thus, the presence of a negative
221 charge at the KSPK motif does not interfere with SQ motif phosphorylation but causes DNA
222 damage sensitivity. These results suggested that serine phosphorylation of KSPK must be
223 prevented to execute DDR.

224 What are the factors preventing phosphorylation of KSPK in H2A.W.7? We
225 hypothesized that the pattern of expression of H2A.W.6 and H2A.W.7 are different leading to
226 expose these two variants to contrasting activities that deposit and maintain KSPK
227 phosphorylation. Contrary to our hypothesis, we observed that KSPK phosphorylation in
228 H2A.W.7 was still absent even when expressed under the control of the promoter of H2A.W.6
229 in the *hta7* mutant (Fig 4D). Residues surrounding the KSPK motifs are distinct between
230 H2A.W.6 and H2A.W.7. Consistently, we observed phosphorylation of KSPK of the C-
231 terminal tail of H2A.W.6 when fused to the core of H2A.W.7 (Fig 4D). This suggested that the
232 primary sequence of the C-tail of H2A.W.6, but not of H2A.W.7, is prone to be phosphorylated
233 *in planta*.

234 **Cross talk between phosphorylation at the KSPK is mediated by proteins containing a**
235 **BRCT domain that binds to phosphorylated SQ**

236 To further investigate a potential crosstalk between phosphorylation of the H2A.W.7 SQ and
237 KSPK motifs, we took a synthetic approach using the fission yeast *Schizosaccharomyces*

238 *pombe*. Fission yeast possesses a relatively reduced repertoire of histone H2A variants,
239 consisting of two H2A.X variants (*Sp*H2A.α and *Sp*H2A.β) and H2A.Z [54, 55]. We modified
240 both genes encoding *Sp*H2A by inserting the C-terminal tail of the *Arabidopsis* H2A.W.6 to the
241 C-terminus of *Sp*H2A.α and *Sp*H2A.β that contains an SQ motif, and obtained the chimeric
242 histone *Sp*H2A.W^{At} that possesses the motifs present in H2A.W.7 [25] (Fig 5A, S5B Fig). In
243 dividing cells, *Sp*H2A.W^{At} localized to the nucleus and was incorporated in chromatin (Fig 5B,
244 S5C Fig). We detected phosphorylation of *Sp*H2A.W^{At} at the KSPK motif but not in a control
245 strain that expressed *Sp*H2A.W^{At} where KSPK was substituted by four alanine residues
246 (*Sp*H2A.W4A^{At}) (Fig 5A and 5C). Interestingly, phosphorylation at the KSPK and SQ motifs
247 were both detected on *Sp*H2A.W^{At} by mass spectrometry (Fig 5E, S5D Fig), demonstrating that
248 *Sp*H2A.W^{At} phosphorylation did not prevent SQ phosphorylation. While the yeast strain
249 expressing *Sp*H2A.W^{At} lacks H2A.X, we predicted that SQ phosphorylation of *Sp*H2A.W^{At}
250 would be sufficient to respond to DNA damage. However, expression of *Sp*H2A.W^{At} caused
251 hyper-sensitivity to DNA damage (Fig 5D). This suggested that either extension of the C-
252 terminal tail or modification of the KSPK motif interfered with the DDR normally mediated by
253 phosphorylation of the SQ motif. To test these two possibilities, we examined DNA damage
254 sensitivity of strains expressing either *Sp*H2A.W^{At}, the KSPQ mutant *Sp*H2A.W4A^{At}, *Sp*H2A
255 with a repeated wild type C-terminal tail (*Sp*H2ACT; contains two SQ motifs) or with alanine
256 substitution of the second SQ motif (*Sp*H2ACT-AA) (Fig 5A). Phosphorylation of the SQ
257 motifs was detected in all strains and none of these modifications resulted in sensitivity to DNA
258 damage treatment, except for *Sp*H2A.W^{At} cells (Fig 5D, S5D Fig). We thus concluded that the
259 mere extension of the C-terminal tail is not responsible for the increased sensitivity to DNA
260 damage in the strain expressing *Sp*H2A.W^{At}.

261 The alternative possibility is that phosphorylation of the KSPK motif specifically
262 interfered with DDR events downstream of SQ phosphorylation. We performed an SGA

263 (synthetic gene array) screen with a genome-wide mutant library of non-essential genes to
264 identify candidate genes that display genetic interactions with *Sp*H2A.W^{At} in presence of the
265 drug hydroxy urea (HU). From the cluster analysis, cluster 2 contained several groups of genes
266 genetically interacting with *Sp*H2A.W^{At}, including S/T protein kinases, S/T phosphatases and
267 DNA repair proteins including BRCT domain proteins (Fig S6). We focused on the BRCT
268 domain protein Mdb1 that binds to phosphorylated SQ motif in fission yeast [19]. Previous
269 studies showed that the phosphorylated SQ motif of *Sp*H2A was able to directly bind Mdb1
270 [19]. To address directly whether presence and/or phosphorylation of KSPK motif interferes
271 with the interaction between Mdb1 and SQ phosphorylation, we performed *in vitro* pull-down
272 assay with synthetic biotinylated peptides (Fig 6A) and recombinant Mdb1. Mdb1 was pulled
273 down by the phosphorylated *Sp*H2A SQ peptide (SpQ) but not by the unmodified version (Fig
274 6A). Surprisingly, Mdb1 was able to bind the phosphorylated SQ motif in the presence of the
275 KSPK motif but not if this latter motif was phosphorylated (Fig 6A). We concluded that
276 phosphorylation of the KSPK motif specifically interfered with DDR events downstream of SQ
277 phosphorylation and likely prevented binding of Mdb1 to the phosphorylated SQ motif (Fig
278 6B).

279 **Discussion**

280 In addition to the well-characterized modifications associated with histone H3, we
281 report a series of modifications at the N- and C-terminal tails, which are either common and
282 specific to the H2A.W family or specific to each isoform. H2A.W.6 is phosphorylated at the
283 serine residue in the KSPK motif in a cell cycle-dependent manner. The kinase CDKA;1, which
284 is active during S phase, is the primary writer of H2A.W.6p, but this mark might also be
285 reinforced by plant specific B-type CDKs active at the G2/M-phase transition [48, 49, 53].
286 When we compare modifications in H2A variants in *Arabidopsis* with other species, we find
287 that some are plant-specific while others are found in other eukaryotes and show interesting

288 parallels. Like S145 that is specific to H2A.W, S95 is only present in H2A and H2A.X in land
289 plants. Phosphorylation of S95 of the replicative H2A variant has been observed in *Arabidopsis*
290 and implicated in flowering time regulation [56]. Certain isoforms of H2A.W in maize are
291 phosphorylated at S133 during mitosis and meiosis [57]. This residue corresponds to S129 of
292 *Arabidopsis* H2A.W and is absent from H2A.Z, H2A.X, and three out of four H2As. In yeast,
293 the corresponding S121 is phosphorylated by Bub1 to recruit shugoshin, an important step for
294 centromere function in chromosome segregation [58-60]. This serine is replaced by threonine
295 (T120) in human H2A and H2A.X, and its phosphorylation is associated with transcriptional
296 activation and mitotic chromosome segregation [61-63]. Consistent with these data, we detected
297 only a few events of S129 phosphorylation in H2A.W in samples originating from leaves or
298 seedlings that contain low amounts of dividing cells. The neighboring lysine 119 of H2A and
299 corresponding lysines of H2A.X, H2A.Z, and macroH2A are well-known ubiquitination sites,
300 associated with transcriptional repression, gene silencing, and DDR [7, 64-72].

301 Surprisingly, although KSPK of H2A.W.7 could be phosphorylated *in vitro*, this
302 modification on H2A.W.7 did not occur *in planta*. We showed that prevention of KSPK
303 phosphorylation in H2A.W.7 originates from the sequence of the C-terminal tail of H2A.W.7
304 and not from its transcriptional pattern. We can speculate that *in planta*, specific modifications
305 of the C-terminal tail of H2A.W.7 prevent the action of the cyclin dependent kinases. We
306 addressed the biological significance of the lack of KSPK phosphorylation on H2A.W.7 *in*
307 *planta* with a synthetic approach by engineering the endogenous H2A from *S. pombe* to create
308 a histone variant analogous to H2A.W.7. The association of both SQ and KSPK motifs in the
309 C-terminal tail of yeast H2A.X resulted in DNA damage sensitivity, highlighting
310 incompatibility of such association. Results obtained *in vitro* indicate that the phosphorylation
311 of the KSPK (S145) motif prevents BRCT domain protein Mdb1 binding to γH2A.X in
312 response to DNA damage. Transgenic *Arabidopsis* plants expressing combinations of
313 phosphomimetic mutants in the SQ and KSPK motifs further supported this conclusion. We

314 propose that phosphorylation of S145 KSPK prevents the recognition of the phosphorylated SQ
315 motif of H2A by an ortholog of Mdb1, which is still unknown in plants. Recruitment of the SQ
316 motif occurred in members of the H2A.W family in various unrelated species during the
317 evolution of flowering plants, suggesting that the mechanism that we describe in *Arabidopsis*
318 has evolved several times and uses pre-existing components from the DDR and cell cycle.

319 Altogether our data illustrate that H2A variants extend the histone modification
320 repertoire across eukaryotes beyond that of the extensively studied H3. Importantly, because
321 H2A strongly impact nucleosome and chromatin properties, H2A variant specific modifications
322 and their interplay extend the potential to modulate these properties, adding a new important
323 layer of epigenetic complexity. Furthermore, through the example of interference between
324 PTMs of motifs of H2A.X and of H2A.W, our findings provide a clue to explain why C-terminal
325 motifs that identify classes of H2A variants are mutually exclusive. We propose that PTMs of
326 these motifs mediate all or part of the function of the motifs themselves. The presence of two
327 motifs side by side might interfere with the function of each motif, leading the emergence of
328 distinct classes of H2A variants differentiated by specific functional motifs with distinct
329 biological functions.

330 **Methods**

331 **Plant material**

332 The mutant lines *hta6* (SALK_024544.32; *h2a.w.6*), *hta7* (GK_149G05; *h2a.w.7*), and *hta12*
333 (SAIL_667_G10; *h2a.w.12*) have been published [21]. Transgenic lines expressing WT and
334 hypomorphic SQ motif mutants of H2A.W.7 in the *hta7* mutant background have been
335 published [16]. The hypomorphic CDKA;1 D and DE mutants [51, 52] and transgenic line
336 expressing CDKA;1-YFP in *cdka;1* mutant background [73] were a kind gift from Dr. Arp
337 Schnittger. Primers used for genotyping hypomorphic CDKA;1 D and DE mutants (S4C Fig)
338 were: Tg9WT/TDNA_N049 (TGTACAAGCGAATAAAGACATTTGA), Tg9WT_N048

339 (CAGATCTCTTCCTGGTTATTCACA), and Tg9TDNASalk_LB_J504
340 (GCGTGGACCGCTTGCTGCAACTCTCTCAGG). Unless otherwise stated, plants were
341 grown in a fully automated climate chamber at 21ºC, under long day conditions.
342 To construct mutant versions of H2A.W.7 containing either WT SQ motif or mutated
343 SQ motif into AQ in combination with phosphomimic and nonphosphorylatable versions of the
344 KSPK motif (KDPK or KAPK, respectively), a two-step PCR reaction was performed using
345 previously described constructs expressing H2A.W.7 containing either the WT SQ or mutated
346 AQ motif [16] as templates. For the first step amplification, the following primer pairs were
347 used: W7-fw (GTACTCTAGAGAGGCATAGATACCGCGCCATC) with either W7-
348 Rev1KDP (AGGATCTTTGGTAGCAGAAG) or W7-Rev1KAP
349 (AGGAGCTTTGGTAGCAGAAG). The second PCR step used the W7-Rev2KDP
350 (AGCAGGATCCAGCCTTCTTAGGATCTTTGGT) or W7-Rev2KAP
351 (AGCAGGATCCAGCCTTCTTAGGAGCTTTGGT) as reverse primers with the same
352 forward primer as above. The mutant *HTA7* fragments were cut with *Bam*HI and *Xba*I and
353 ligated into pCBK02. *hta7* mutant plants were transformed by the floral dip method and
354 transgenic plants were selected on MS plates containing 10 µg/ml of phosphinothricin. The T3
355 and T4 homozygous seeds containing single transgene copy were used for experiments.
356 For swapping the promotors and tails of H2A.W.6 and H2A.W.7, cloning primers (S1 Table)
357 were used to amplify the different fragments from genomic DNA of *Arabidopsis* seedlings. We
358 created the green gate entry modules following previously published protocol [74]. The
359 promotor fragments were introduced into the A-B empty vector, the full H2A.W.6 and
360 H2A.W.7 as well as the N-terminal+core fragments were introduced into the C-D empty vector
361 and the tail fragments were introduced into the D-E empty vectors. The Ub10 Terminator in the
362 E-F entry vector and the selection based on seed coat YFP fluorescence were a gift from Yasin
363 Dagdas laboratory. For the final greengate reaction pGGZ003_ccdB, the entry clones were
364 combined with empty destination vector. The final constructs were transformed into the triple

365 *hta6 hta7 hta12* mutant which is a complete knock-out line deprived of H2A.W described in
366 the preprint doi: https://doi.org/10.1101/2020.03.19.998609.
367 .

368 **Isolation of nuclei, micrococcal nuclease (MNase) chromatin digestions,**
369 **immunoprecipitation, and SDS-PAGE**

370 Nuclei isolation, MNase digestion, and immunoprecipitation were performed as previously
371 described [16] by using 4 grams of 2-3 week old leaves for each antibody. Isolated nuclei were
372 washed once in 1 ml of N buffer (15 mM Tris-HCl pH 7.5, 60 mM KCl, 15 mM NaCl, 5 mM
373 $MgCl_2$, 1 mM $CaCl_2$, 250 mM sucrose, 1 mM DTT, 10 mM ß-glycerophosphate) supplemented
374 with protease and phosphatase inhibitors (Roche). After centrifuging for 5 min at 1,800 × *g* at
375 4ºC, nuclei were re-suspended in N buffer to a volume of 1 ml. Twenty µl of MNase (0.1 u/µl)
376 (SigmaAldrich) were added to each tube and incubated for 15 min at 37ºC. During the
377 incubation, nuclei were mixed 4 times by inverting the tubes. MNase digestion was stopped on
378 ice by the addition of 110 µl of MNase stop solution (100 mM EDTA, 100 mM EGTA). Nuclei
379 were lysed by the addition of 110 µl of 5 M NaCl (final concentration of 500 mM NaCl). The
380 suspension was mixed by inverting the tubes and they were then kept on ice for 15 min. Extracts
381 were cleared by centrifugation for 10 min at 20,000 × *g* at 4ºC. Supernatants were collected and
382 centrifuged again as above. For each immunoprecipitation extract, an equivalent of 4 g of leaf
383 material was used, usually in a volume of 1 ml. To control MNase digestion efficiency, 200 µl
384 of the extract were kept for DNA extraction. Antibodies, including non-specific IgG from
385 rabbit, were bound to protein A magnetic beads (GE Healthcare) and then incubated with
386 MNase extracts over night at 4ºC. Beads were washed 2 times with N buffer without sucrose
387 containing 300 mM NaCl, followed by 3 washes with N buffer containing 500 mM NaCl
388 without sucrose, and 1 wash with N buffer without sucrose, containing 150 mM NaCl. Beads
389 were incubated 2 times with 15 µl of hot loading buffer for 5 min and supernatants were

390 removed and combined. Proteins were resolved on 4-20% gradient gels (Serva) and silver
391 stained.

392 **Generation of antibodies, isolation of nuclei, SDS-PAGE, and western blotting**

393 Antibodies against H2A.X, H2A.W.6, H2A.W.7, γH2A.X, and γH2A.W.7 have been described
394 [16, 21]. Antibodies against the H2A.W.6 phosphopeptide (CEEKATKSPVKSpPKKA) were
395 raised in rabbits (Eurogentec) and purified by peptide affinity column. Purified IgG fractions
396 were tested for specificity on peptide arrays containing serial dilutions of non-phosphorylated
397 and phosphorylated peptides (phospho-serine specific antibodies).

398 Nuclei for western blot analyses were prepared from 300 mg of tissue (10-12 day old
399 treated seedlings) as described [16]. Tissue was frozen in liquid nitrogen and disrupted in 15
400 ml Falcon tubes by rigorous vortexing with 5 small ceramic beads. Ten ml of nuclei isolation
401 buffer (NIB; 10 mM MES-KOH pH 5.3, 10 mM NaCl, 10 mM KCl, 250 mM sucrose, 2.5 mM
402 EDTA, 2.5 mM ß-mercaptoethanol, 0.1 mM spermine, 0.1 mM spermidine, 0.3% Triton X-
403 100), supplemented with protease and phosphatase inhibitors (Roche) were added followed by
404 short vortexing to obtain a fine suspension. The suspension was filtered through 2 layers of
405 Miracloth (Merck Millipore) into 50 ml Falcon tubes, followed by washing the Miracloth with
406 NIB. The sample was centrifuged at 3,000 rpm for 5 min at 4°C. The pellet was resuspended in
407 NIB buffer and transferred into an Eppendorf tube. The sample was centrifuged for 2 min at
408 4°C at full speed and the resulting pellet was resuspended in 0.3 × PBS in 1 × Laemmli loading
409 buffer. The sample was then boiled for 5 min and immediately centrifuged for 2 min at
410 maximum speed to remove starch and other large particles. For western blot analyses, 10 µl for
411 histone variants, 20 µl for histone modifications, and 10 µl for H3, used as a loading control,
412 were loaded per lane. Western blots with phospho-specific antibodies were performed in
413 solutions containing TBS instead of PBS and, after blocking, the membranes were incubated
414 with primary antibody in TBS without milk.

415 Antibodies against H2A.X, H2A.W.6, H2A.W.7, γH2A.X, and γH2A.W.7 [16, 21], as
416 well as H2A.W.6p (this work), H3 (ab1791, Abcam), CDK (PSTAIR, Sigma P7962), and
417 CDKY15p (Cell Signaling Technology) were used at 1:1,000 dilution and secondary
418 antibodies, HRP conjugated goat anti-rabbit and goat anti-mouse, at 1:10,000. Signals were
419 detected using the chemiluminescence kit (ThermoFisher), recorded using an ImageDoc
420 instrument (BioRad), exported to Photoshop, and prepared for publication. Quantification of
421 western blots was done with ImageLab 5.2 software (BioRad) using the volume tool. For
422 detection of Y15 phosphorylation of CDK, the manufacturer's protocol was followed.

423 **Nano LC-MS/MS analysis**

424 Histone bands corresponding to H2A.W.6/H2A.W.7 from *Arabidopsis* and
425 *Sp*H2A/*Sp*H2A.W/*Sp*H2A.W4A from fission yeast were excised from silver stained gels,
426 reduced, alkylated, in-gel trypsin, LysC, and subtilisin digested, and processed for MS. The
427 nano HPLC system used was a Dionex UltiMate 3000 HPLC RSLC (Thermo Fisher Scientific,
428 Amsterdam, Netherlands) coupled to a Q Exactive HF mass spectrometer (Thermo Fisher
429 Scientific, Bremen, Germany), equipped with a Proxeon nanospray source (Thermo Fisher
430 Scientific, Odense, Denmark). Peptides were loaded onto a trap column (Thermo Fisher
431 Scientific, Amsterdam, Netherlands, PepMap C18, 5 mm × 300 µm ID, 5 µm particles, 100 Å
432 pore size) at a flow rate of 25 µl/min using 0.1% TFA as the mobile phase. After 10 min, the
433 trap column was switched in line with the analytical column (Thermo Fisher Scientific,
434 Amsterdam, Netherlands, PepMap C18, 500 mm × 75 µm ID, 2 µm, 100 Å). Peptides were
435 eluted using a flow rate of 230 nl/min, and a binary 1-hour gradient.

436 The Q Exactive HF mass spectrometer was operated in data-dependent mode, using a
437 full scan (m/z range 380-1500, nominal resolution of 60,000, target value 1E6) followed by
438 MS/MS scans of the 10 most abundant ions. MS/MS spectra were acquired using normalized
439 collision energy of 27%, isolation width of 1.4 m/z, resolution of 30,000 and the target value

440 was set to 1E5. Precursor ions selected for fragmentation (exclude charge state 1, 7, 8, >8) were
441 put on a dynamic exclusion list for 20 s. Additionally, the minimum AGC target was set to 5E3
442 and intensity threshold was calculated to be 4.8E4. The peptide match feature was set to
443 preferred and the exclude isotopes feature was enabled. For peptide identification, the RAW
444 files were loaded into Proteome Discoverer (version 2.1.0.81, Thermo Scientific). All hereby
445 created MS/MS spectra were searched using Mascot 2.2.7 against a database which contains all
446 histone variants from *Arabidopsis thaliana*. The following search parameters were used: Beta-
447 methylthiolation on cysteine was set as a fixed modification, oxidation on methionine,
448 deamidation on asparagine and glutamine, acetylation on lysine, phosphorylation on serine,
449 threonine and tyrosine, methylation and di-methylation on lysine and arginine and tri-
450 methylation on lysine were set as variable modifications. Monoisotopic masses were searched
451 within unrestricted protein masses for tryptic enzymatic specificity. The peptide mass tolerance
452 was set to ±5 ppm and the fragment mass tolerance to ±0.03 Da. The result was filtered to 1%
453 FDR at the peptide level using the Percolator algorithm integrated in Thermo Proteome
454 Discoverer and additional a minimum Mascot score of 20. In addition, we have checked the
455 quality of the MS/MS spectra manually. The localization of the phosphorylation sites within
456 the peptides was performed with ptmRS using a probability threshold of minimum 75 [75].

457 **DNA damage sensitivity assays**

458 For the true leaf assay, sterilized seeds were put on MS plates containing 50 µg/ml of zeocin
459 (Invitrogen) and, after stratification at 4ºC for 3 days, germinated under long day conditions.
460 Development of true leaves was scored 12 days after germination. For analysis of H2A.W.7,
461 H2A.X, and H2A.W.6 phosphorylation in response to DNA damage, 300 mg of twelve-day old
462 seedlings germinated and grown on MS plates under long day conditions were treated in liquid
463 MS medium with 20 µg/ml bleomycin (Calbiochem) for the indicated time periods or for 2

464 hours with 20 µg/ml bleomycin. After treatment, seedlings were removed from medium and
465 shock frozen in liquid nitrogen for nuclei isolation and western blot analysis as described above.

466 **Cell cycle synchronization of BY-2 cell suspension culture with aphidicolin**

467 The BY-2 cell suspension culture was sub-cultured every 2 weeks by adding 1 ml of the
468 previous culture to 50 ml fresh BY-2 media. The culture was kept in the dark and under constant
469 shaking at 130 rpm at room temperature. For cell cycle synchronization, a previously published
470 protocol was followed [76]. In short, 1.5 ml of stationary BY-2 cells were added to 95 ml of
471 fresh BY-2 media and grown for 5 days at 27°C. This culture was diluted 4 times with fresh
472 BY-2 media and then treated with 20 µg/ml aphidicolin (1 mg/ml; SigmaAldrich) for 24 hours
473 at 27°C to reach a cell cycle block. To release the cells from this block, the cells were passed
474 over a 40 µm sieve, washed with fresh media, and resuspended in 100 ml of fresh media and
475 followed in a time course of 12 hours. Every hour, a sample was taken for western blotting and
476 flow cytometry analysis. For western blotting, 5 ml of cells were collected with a 50 µm sieve
477 and immediately frozen in liquid nitrogen. To extract proteins, samples were crushed with a
478 small pistil in an Eppendorf tube and mixed with 200-250 µl of 1 × loading buffer in 1 × PBS.
479 Samples were boiled for 5 min at 99°C followed by centrifugation at full speed for 5 min.
480 Fifteen µl were loaded onto 15% SDS-PAGE gels and analyzed by western blotting.

481 For the flow cytometry analysis, 2 ml of cells were collected with a 50 µm sieve. The
482 cells were resuspended in a small Petri dish in 400 µl of extraction buffer (CyStain UV Precise
483 P kit from Sysmex) and chopped with a razor blade. The sample was transferred onto a 50 µm
484 CellTrics Disposable filter (Partec), placed on top of a flow cytometry tube, and 1,5 ml of DAPI
485 stain solution (CyStain UV Precise P kit from Sysmex) was added to the sieve. The samples
486 were then analyzed by the Partec flow cytometer with a gain set to 380.

487 **Staining of *Arabidopsis* roots with EdU**

488 For the whole mount EdU staining and immunostaining with the phosphorylation specific
489 antibody in roots, the protocol for the Click-iT EdU imaging kit from Invitrogen was combined

490 with the protocol from [77]. *Arabidopsis* plants were grown on MS plates for 1 week and fifteen
491 seedlings were incubated for 1 hour in liquid MS media containing 10 μM EdU at room
492 temperature. The seedlings were washed twice with MS media to remove the EdU. The roots
493 were cut off and transferred into an Eppendorf tube with fixative solution, incubated for 1 hour
494 at room temperature, and washed twice for 10 min with 1×PBS and twice for 5 min with water.
495 The roots were transferred to the microscope slide and allowed to dry. The material was then
496 rehydrated by adding 1 × PBS for 5 min followed by incubation with 2% driselase (Sigma) for
497 60 min at 37°C in a moisture chamber to remove the cell wall. The roots were washed 6 times
498 for 5 min with 1×PBS at room temperature. Mixture of 3% IGEPAL CA-630 plus 10% DMSO
499 was added to the slide and incubated for 60 min at room temperature. The solution was
500 removed, and the slides were washed 8 times with 1 × PBS for 5 min. The slides were then
501 incubated with 3% BSA in 1 × PBS for 5 min before revealing EdU incorporation with the
502 Click-iT reaction buffer. After this reaction, the slides were washed once for 5 min with 3%
503 BSA in 1 × PBS followed by blocking for 60 min at room temperature with 3% BSA in 1 ×
504 PBS. Approximately 150 μl of the primary antibody diluted 1:100 in 3% BSA 1 × PBS was
505 added to the slides and incubated for 4 hours at 37°C in a humid chamber and then overnight at
506 4°C. Before incubating with the secondary antibody, the slides were washed 5 times with 1 ×
507 PBS for 10 min at room temperature. Alexa flour 555 labelled goat anti-rabbit IgG (Life
508 Technologies) diluted 1:200 in 1 × PBS containing 3% BSA was added to slides and incubated
509 for 3 hours at 37°C in a humid chamber. Finally, slides were again washed 5 times for 10 min
510 with 1 × PBS at room temperature and mounted in Vectashield (Vector Laboratories) with 1
511 μg/ml DAPI. Slides were examined on an LSC confocal microscope (Carl Zeiss) and confocal
512 sections were acquired with a 40 × oil objective, exported to Adobe Photoshop, and prepared
513 for publication.

514 **Treatment of *Arabidopsis* cell suspension with cell cycle inhibitors**

515 The T87 cell suspension was grown on a shaker at 130 rpm under constant light. For treatment
516 with different cell cycle inhibitors, 5 ml of the 7-day old culture were mixed with 5 ml of fresh
517 BY-2 media supplemented with the indicated amounts of the inhibitors. The concentrations that
518 were used for the treatment were: 50 µM roscovitine (50 mM solution from Merck); 10 mM
519 hydroxyurea (SigmaAldrich); 4 µg/ml aphidicolin (SigmaAldrich). Cells were incubated with
520 the inhibitors for 24 hours and subsequently collected by removing the media with a 50 µm
521 mesh, shock frozen in liquid nitrogen, and stored at -80°C.

522 For treatment of cell suspension cultures with different concentrations of roscovitine, a
523 7-day old *Arabidopsis* T87 culture was diluted in BY-2 media to an OD_{600} of 0.167. 10 ml of
524 the diluted culture were incubated for 24 hours with or without 10 µM, 20 µM, 30 µM, 40 µM,
525 and 50 µM roscovitine with shaking under constant light. Seven ml of each sample were
526 collected, and the cells were disrupted with ceramic beads and immediately mixed with 1 ×
527 Laemmli loading buffer in 0.3 × PBS without prior enrichment of nuclei.

528 **Immunoprecipitation of CDKA;1 from *cdka-/-* CDKA;1::YFP plants**

529 For immunoprecipitation, 1.5 g of 15 day old CDKA;1::YFP *cdka-/-* [73] and WT seedlings
530 grown on MS plates were crushed in liquid nitrogen and powder was resuspended in PEB400
531 buffer (50 mM HEPES-KOH pH 7.9, 400 mM KCl, 1 mM DTT, 2.5 mM $MgCl_2$, 1 mM EDTA,
532 0.1% Triton X-100) [78] supplemented with protease inhibitor cocktail (Roche) (100 µl of
533 buffer per 100 mg of seedlings) and the suspension was incubated on ice for 10 minutes. The
534 samples were centrifuged for 10 min at full speed at 4°C. The supernatants were transferred to
535 a new tube and centrifuged as above. The volume of the sample was measured and the same
536 volume of PEB buffer without KCl was added to obtain the PEB buffer with 200 mM KCl. At
537 this step, an input aliquot was taken and mixed with 5 × loading buffer. Agarose beads coupled
538 with GFP nanobodies (40 µl; VBC Molecular Biology Services) were washed twice with
539 PEB200 and the protein extracts were added to the beads and the mixture was incubated
540 overnight at 4°C on a rotating wheel. The beads were washed 3 times with 1 ml of PEB200

541 followed by 2 washes with kinase buffer (20 mM Tris-HCl pH7.5, 50 mM KCl, 5 mM $MgCl_2$,
542 1 mM DTT) if they were used for the *in vitro* kinase assay. To analyze immunoprecipitations
543 by SDS-PAGE and western blotting, 30 µl of 1 × loading buffer in PEB200 were added to the
544 beads. After boiling for 5 min, the supernatants were loaded onto a 12% SDS-PAGE gel.

545 ***In vitro* phosphorylation assay**

546 For the kinase assay, 10 µl of kinase buffer were added to the agarose beads with the
547 immunoprecipitated CDKA;1-YFP. One µg of the reconstituted histone dimers (H2A.W.6-
548 H2B.9, H2A.W.7-H2B.9, H2A.13-H2B.9) and 200 µM ATP were added and the reaction was
549 mixed before incubating for 35 min at 30°C. As a control, 20 µl kinase buffer were mixed with
550 the dimers and ATP for 35 min at 30°C. Reactions were stopped by adding 5× loading buffer
551 and analyzed by SDS-PAGE followed by western blotting with H2A.W.6p antibody.

552 **Cloning of H2A.W.7 into overexpression vector pET15b**

553 cDNA encoding H2A.W.7 was PCR amplified from a seedling cDNA library using the
554 following primers: W7pET15bfor (GCATCCATATGGAGTCATCACAA) and W7pET15brev
555 (CTAATGGATCCTCAAGCCTTCTT). The PCR product was cleaned using the PCR
556 purification kit from Qiagen, digested with *Nde*I/*Bam*HI, gel purified, and ligated into
557 *Nde*I/*Bam*HI opened pET15b (Novagene). Plasmids for expression of His-tagged H2A.W.6,
558 H2A.13, and H2B.9 have been published [21, 22].

559 **Overexpression and purification of recombinant histones and assembly of H2A-H2B**
560 **dimers**

561 Proteins were overexpressed in *E. coli* BL21 (DE3) overnight at 37°C. Histone purification was
562 performed as previously described [79, 80]. Cells pellets were resuspended in sonication buffer
563 1 (50 mM Tris-HCl pH8.0, 500 mM NaCl, 1 mM PMSF, 5% glycerol) and sonicated with 50%
564 power for 5 min. After centrifugation at 15,000 rpm at 4°C for 20 min, pellets were resuspended
565 in sonication buffer 1 and sonicated at 35% power for 2 min followed by centrifugation as
566 before. The resulting pellets were resuspended in sonication buffer 2 (50 mM Tris-HCl pH 8.0,

567 500 mM NaCl, 7 M guanidine hydrochloride, 5% glycerol) and sonicated as described before.
568 After the third sonication, the suspension was rotated at 4°C overnight. After centrifugation,
569 the supernatants containing denatured proteins were mixed with Ni-NTA resin (Qiagen) and
570 incubated for 60 min at 4°C. To remove the supernatant, the suspension was centrifuged. The
571 resin was resuspended in wash buffer (50 mM Tris-HCl pH8.0, 500 mM NaCl, 6 M urea, 5%
572 glycerol, 5 mM imidazole) and transferred into an Econo-column (BioRad). After washing with
573 50 column volumes of wash buffer, proteins were eluted with elution buffer (50 mM Tris-HCl
574 pH8.0, 500 mM NaCl, 6 M urea, 5% glycerol, 500 mM imidazole) and collected in 2 ml
575 fractions. The fractions were analyzed on a 15% SDS-PAGE gel and those containing histones
576 were pooled together and dialyzed against 4L of 10 mM Tris-HCl pH 7.5, 2 mM 2-
577 mercaptoethanol at 4°C for 2 days. After checking the thrombin cleavage efficiency with
578 different U/mg of thrombin, the estimated amount of thrombin was added to each sample and
579 incubated for 3 hours at room temperature followed by analysis on a 15% SDS-PAGE gel.
580 Proteins were further purified by cation ion exchange chromatography. The sample was applied
581 to an SP sepharose column (GE Healthcare) connected to an Äkta system. The column was
582 equilibrated and washed with equilibration buffer (20 mM CH_3COONa pH5.2, 200 mM NaCl,
583 6 M urea, 5 mM 2-mercaptoethanol, 1 mM EDTA). For elution, a linear gradient of 200-800
584 mM NaCl in elution buffer (20 mM CH_3COONa pH 5.2, 6 M urea, 5 mM ß-mercaptoethanol,
585 1 mM EDTA) was used. The fractions were again analyzed on a 15% SDS-PAGE gel. Histone
586 containing fractions were pooled together and dialyzed against 4 L of 2 mM 2-mercaptoethanol
587 4 times for 4 hours. Finally, the purified histones were freeze-dried.

588 For histone H2A-H2B dimer reconstitution, freeze-dried histones were resolved in
589 unfolding buffer (20 mM Tris-HCl pH 7.5, 7 M guanidine hydrochloride, 20 mM 2-
590 mercaptoethanol) at a concentration of 1 mg/ml at a 1:1 molar ratio and incubated for 2 hours
591 at 4°C on a wheel. Samples were step-wise dialyzed against refolding buffer (20 mM, Tris-HCl
592 pH 7.5, 1 mM EDTA, 0.1 M PMSF, 5%glycerol, 5 mM 2-mercaptoethanol) staring with 2 M

593 NaCl at 4°C overnight, followed by 1 M NaCl refolding buffer at 4°C for 4 hours, 0.5 M NaCl
594 refolding buffer at 4°C for 4 hours, and finally against 0.1 M NaCl refolding buffer at 4°C
595 overnight. Proteins were concentrated by centrifugation with a 10 kDa cut-off membrane
596 (Merck Millipore) to a volume of 300 µl. The sample was applied to a Superdex200 gel
597 filtration column in 0.1 M NaCl refolding buffer. Peak fractions were analyzed on a 15% SDS-
598 PAGE gel and fractions containing the heterodimers were pooled together. The heterodimers
599 were then concentrated by ultrafiltration (10 kDa cut-off) and, at the same time, the buffer was
600 exchanged to kinase buffer. The final protein concentration was determined by measuring the
601 absorbance at 280 nm and the quality was analyzed on a 15% SDS-PAGE gel.

602 ***Schizosaccharomyces pombe* strains and media**

603 Unless otherwise stated, cells were grown in rich medium (YES). Gene replacement and
604 tagging were performed by homologous recombination using a plasmid-based method [81]. The
605 primers used are listed in S1 Table. In brief, pCloneNat1 and pCloneHyg1 were used to fuse
606 the H2A.W.6 (*At*) C-terminal 21 amino acids to the endogenous C-terminus of *Sp*H2A.α and
607 *Sp*H2A.β by using the natMX4 or hphMX4 cassette, respectively [25]. All constructed strains
608 in this study were verified by PCR analysis and sequencing.

609 ***S. pombe* chromatin fractionation assay**

610 Chromatin fractionation of WT and *Sp*H2A.W^{At} strains was performed as previously described
611 [82] and fractions were analyzed by western blotting using anti-αtubulin (T6199, Sigma), anti-
612 H3 (ab1791, Abcam), and anti-H2A.W.6 (antibodies recognizing C-terminal KSPKKA motif).

613 **Preparation of *S. pombe* whole cell extracts and acid extraction of histones for MS analysis**

614 Cells were disrupted by 0.5 mm glass beads in lysis buffer (50 mM Tris-HCl pH 7.5, 150 mM
615 NaCl, 5 mM EDTA, 10% glycerol and 1 mM PMSF) and centrifuged at 14,000 × *g* for 15 min
616 at 4°C. Supernatant was collected as a whole cell extract. Histones were analyzed by western
617 blotting with antibodies against fission yeast-specific phosphoS129 of H2A (ab17353, Abcam),
618 H2A.W.6p, and H3 (ab1791, Abcam). For mass spectrometry, histones from WT, *Sp*H2ACT,

619 *Sp*H2ACT-AA, *Sp*H2A.W^{At}, and *Sp*H2A.W4A^{At} cells were prepared by the acid extraction and
620 acetone precipitation method [83].

621 **Indirect immunofluorescence on *S. pombe* cells**

622 For detection of *Sp*H2A.W^{At} by immunofluorescence, cells expressing FLAG-tagged
623 *Sp*H2A.W^{At} were fixed with 4% paraformaldehyde, digested to spheroplasts with zymolyase
624 (Zymo Research), permeabilized with 1% Triton X-100, and incubated with an anti-Flag
625 antibody (F1804, Sigma) as the primary antibody at a 1:100 dilution and anti-mouse IgG Alexa
626 Fluor 488 as the secondary antibody (A11029, Life Technologies) at a 1:100 dilution. Cells
627 were placed onto poly L-lysine-coated coverslips and DAPI stained. Microscopic analysis was
628 performed using LSM700 laser scanning confocal microscope (Zeiss).

629 **Sensitivity of *S. pombe* strains to MMS**

630 Cells were grown in YES medium at 32°C until the exponential phase and for all strains the
631 OD_{600} was adjusted to 1.0. Five-fold serial dilutions were made with fresh YES and 2 µl were
632 spotted on YES plates or YES plates containing 0.004% methyl methane sulfonate (MMS) and
633 incubated at 32˚C for 3 days.

634 **Peptide Pull Down assay**

635 6His-tagged Mdb1 recombinant protein was expressed in BL21 and purified using Ni-NTA
636 beads (Qiagen) following manufacturer's instructions. As control, we synthesized two peptides
637 corresponding to residues 120–132 of yeast H2A C-terminal tail, with serine 129 being
638 unphosphorylated (termed as SQ) and phosphorylated (termed as SpQ). The other two peptides
639 corresponding to residues 129–149 of H2A.W6 from *Arabidopsis*, with serine 145 being
640 unphosphorylated (termed as KSPK) and phosphorylated (termed as KSpPK) together with
641 SpQ peptide. All these peptides coupled with biotin at N-terminal. Twenty micrograms of each
642 peptide were incubated with 20 µl of pre-washed Dynabeads M-280 Streptavidin (Invitrogen)
643 at RT for 1 hour, then incubated with purified Mdb1 in peptide binding buffer (50 mM Tris-

644 HCl, pH 7.5, 100 mM NaCl, 0.05% NP-40) at 4°C for overnight. Beads were washed with
645 peptide binding buffer and eluted with SDS loading buffer.

646 **Yeast Genetic interaction screening**

647 Large-scale crosses by SGA (synthetic genetic array) were carried out using the Bioneer haploid
648 deletion mutant library (version 3.0) and the query strains WT and *sp*H2A.W^{At}. Manipulations
649 were performed using a Singer RoToR colony pinning robot, essentially as described previously
650 [84]. First, the library and query strains were arrayed in 384 colony format on YES agar
651 containing 250 µg/ml G418 (Geneticin; Life Technologies, 10131027) or 100 µg/ml ClonNat
652 (Nourseothricin; Jena Bioscience, AB-102XL) and 50 µg/ml Hygromycin B (Invitrogen/Life
653 Technologies, 10687010), respectively. Mating between library and query strains, and selection
654 of progeny was largely performed as previously reported [85]. Briefly, query and library stain
655 cells were mixed in a drop of sterile H_2O on SPAS plates and allowed to sporulate at 24˚C for
656 3 days. The resulting cell/spore mixture was incubated at 42˚C for 7 days to enrich for spores
657 and plated onto selective media to select for haploid progeny bearing the gene deletion and/or
658 *sp*H2A.W^{At}. Finally, the selected haploid progeny was grown YES or YES supplemented with
659 or 9 mM hydroxyurea (Sigma, H8627) at 32˚C. For each individual screen with the WT and
660 *sp*H2A.W^{At} query strains, technical duplicates were processed following the germination step,
661 and each screen was repeated independently at least 3 times, resulting in a total number of n =
662 6 screen for data analysis.

663 **Data analysis of the genetic screen and visualization**

664 SGA analysis was performed as previously described [86], with some modifications. Genetic
665 interactions were assessed by colony growth on YES plates containing no additives (non-
666 selective media; N/S) and YES plates containing formamide or hydroxyurea (treatment) and
667 quantified by determining colony sizes (area) of digitalized pictures. As colonies at the edges
668 of the plates show increased growth due to better availability of nutrients, the size of colonies

669 of the first and second outer most rims was corrected by multiplying with a correction factor.
670 For calculating this factor, we determined the ratio between the median of all colonies in the
671 middle of the plate (i.e., excluding the first and second rims) and the median of the first and
672 second outer most rims. Next, the sensitivity towards stress conditions was determined by
673 calculating the ratio between growth on 'treatment' and 'N/S' for each individual mutant; the
674 obtained value for each mutant was then normalized to the median of the treatment: N/S values
675 derived from all mutants of the same 384-plate. Finally, the entire dataset of each screen was
676 then $\log_2$-transformed and median-normalized to all mutants from the entire screen (array). To
677 select for robust genetic interactions, data from all screens, query strains and stress conditions
678 were filtered to select for those mutants containing at least 80% of present values and show at
679 least 5 absolute values higher or equal to 0.3 ($\log_2$), resulting in the selection of 529 mutants.
680 Next, hierarchical clustering of the genetic interaction dataset was performed using Euclidean
681 distance as the similarity metric and complete linkage as the clustering method using Gene
682 Cluster 3.0. Hierarchical cluster maps were visualized with Java TreeView (version 1.1.6) with
683 negative and positive values represented in blue and yellow, respectively (grey: missing or N/A
684 data).
685

686 **SUPPLEMENTARY DATA**

687 Supplementary Data are available at Journal Online.

688 **FUNDING**

689 FB acknowledges support from the next generation sequencing facilities at the Vienna
690 BioCenter Core Facilities (VBCF), and the BioOptics facility and Molecular Biology Services
691 from the Institute for Molecular Pathology (IMP), and Dr. J. Matthew Watson for proof-reading
692 the manuscript. This work was also supported by the Gregor Mendel Institute (FB) and grant
693 from Fonds zur Förderung der wissenschaftlichen Forschung (FWF) P26887, P28320, P30802,
694 P32054, and TAI304 (BL, ZL and FB), and DK chromatin dynamics W1238 (AS). SB is a

member of the Collaborative Research Center SFB 1064 (Project-ID 213249687) funded by the Deutsche Forschungsgemeinschaft (DFG, German Research Foundation) and acknowledges infrastructural support. SB was supported by a grant by the German Research Foundation (DFG, BR 3511/4-1). The work in the Mechtler lab was financially supported by the EPIC-XS, project number 823839, the Horizon 2020 Program of the European Union, and the ERA-CAPS I 3686 project of the Austrian Science Fund.

Authors contributions

AS, BL and ZL performed experiments, and contributed data. FB, ZL, AS and BL interpreted data and wrote the manuscript. KM contributed Mass spectrometry analysis. MC and SB contributed the genetic screen and participated in revising the manuscript. PB and OM contributed the triple mutant line deprived of H2A.W. FB KM and SB were responsible for supervision.

Acknowledgments

We thank technical assistance from the Vienna Biocenter Core Facilities for Plant Science and the IMP/IMBA/GMI BioOptics and Protein Chemistry facilities for support (Ines Steinmacher, Susanne Opravil, Gabriela Krssakova, Otto Hudecz and Richard Imre).

References

1. Talbert PB, Henikoff S. Histone variants on the move: substrates for chromatin dynamics. Nat Rev Mol Cell Biol. 2017;18(2):115-26. doi: 10.1038/nrm.2016.148. PubMed PMID: 27924075.
2. Talbert PB, Meers MP, Henikoff S. Old cogs, new tricks: the evolution of gene expression in a chromatin context. Nat Rev Genet. 2019. doi: 10.1038/s41576-019-0105-7. PubMed PMID: 30886348.
3. Jiang D, Borg M, Lorkovic ZJ, Montgomery SA, Osakabe A, Yelagandula R, et al. The evolution and functional divergence of the histone H2B family in plants. PLoS Genet. 2020;16(7):e1008964. Epub 2020/07/28. doi: 10.1371/journal.pgen.1008964. PubMed PMID: 32716939; PubMed Central PMCID: PMCPMC7410336.
4. Loppin B, Berger F. Histone Variants: The Nexus of Developmental Decisions and Epigenetic Memory. Annu Rev Genet. 2020;54:121-49. Epub 2020/08/29. doi: 10.1146/annurev-genet-022620-100039. PubMed PMID: 32857637.

5. Buschbeck M, Hake SB. Variants of core histones and their roles in cell fate decisions, development and cancer. Nat Rev Mol Cell Biol. 2017;18(5):299-314. doi: 10.1038/nrm.2016.166. PubMed PMID: 28144029.
6. Filipescu D, Muller S, Almouzni G. Histone H3 variants and their chaperones during development and disease: contributing to epigenetic control. Annu Rev Cell Dev Biol. 2014;30:615-46. doi: 10.1146/annurev-cellbio-100913-013311. PubMed PMID: 25288118.
7. Corujo D, Buschbeck M. Post-Translational Modifications of H2A Histone Variants and Their Role in Cancer. Cancers (Basel). 2018;10(3). doi: 10.3390/cancers10030059. PubMed PMID: 29495465; PubMed Central PMCID: PMCPMC5876634.
8. Dona M, Mittelsten Scheid O. DNA Damage Repair in the Context of Plant Chromatin. Plant Physiol. 2015;168(4):1206-18. Epub 2015/06/20. doi: 10.1104/pp.15.00538

pp.15.00538 [pii]. PubMed PMID: 26089404; PubMed Central PMCID: PMC4528755.
9. Lorkovic ZJ, Berger F. Heterochromatin and DNA damage repair: Use different histone variants and relax. Nucleus. 2017;8(6):583-8. doi: 10.1080/19491034.2017.1384893. PubMed PMID: 29077523; PubMed Central PMCID: PMCPMC5788557.
10. Hauer MH, Gasser SM. Chromatin and nucleosome dynamics in DNA damage and repair. Genes Dev. 2017;31(22):2204-21. doi: 10.1101/gad.307702.117. PubMed PMID: 29284710; PubMed Central PMCID: PMCPMC5769766.
11. Kim JJ, Lee SY, Miller KM. Preserving genome integrity and function: the DNA damage response and histone modifications. Crit Rev Biochem Mol Biol. 2019:1-34. doi: 10.1080/10409238.2019.1620676. PubMed PMID: 31164001.
12. Stucki M, Clapperton JA, Mohammad D, Yaffe MB, Smerdon SJ, Jackson SP. MDC1 directly binds phosphorylated histone H2AX to regulate cellular responses to DNA double-strand breaks. Cell. 2005;123(7):1213-26. doi: 10.1016/j.cell.2005.09.038. PubMed PMID: 16377563.
13. Peng G, Lin SY. BRIT1/MCPH1 is a multifunctional DNA damage responsive protein mediating DNA repair-associated chromatin remodeling. Cell Cycle. 2009;8(19):3071-2. doi: 10.4161/cc.8.19.9411. PubMed PMID: 19755841; PubMed Central PMCID: PMCPMC3419473.
14. Peng G, Yim EK, Dai H, Jackson AP, Burgt I, Pan MR, et al. BRIT1/MCPH1 links chromatin remodelling to DNA damage response. Nat Cell Biol. 2009;11(7):865-72. doi: 10.1038/ncb1895. PubMed PMID: 19525936; PubMed Central PMCID: PMCPMC2714531.
15. Sawicka A, Seiser C. Sensing core histone phosphorylation - a matter of perfect timing. Biochim Biophys Acta. 2014;1839(8):711-8. doi: 10.1016/j.bbagrm.2014.04.013. PubMed PMID: 24747175; PubMed Central PMCID: PMCPMC4103482.
16. Lorkovic ZJ, Park C, Goiser M, Jiang D, Kurzbauer MT, Schlogelhofer P, et al. Compartmentalization of DNA Damage Response between Heterochromatin and Euchromatin Is Mediated by Distinct H2A Histone Variants. Curr Biol. 2017;27(8):1192-9. doi: 10.1016/j.cub.2017.03.002. PubMed PMID: 28392109.
17. Redon C, Pilch DR, Rogakou EP, Orr AH, Lowndes NF, Bonner WM. Yeast histone 2A serine 129 is essential for the efficient repair of checkpoint-blind DNA damage. EMBO Rep. 2003;4(7):678-84. Epub 2003/06/07. doi: 10.1038/sj.embor.embor871. PubMed PMID: 12792653; PubMed Central PMCID: PMCPMC1326317.
18. Sofueva S, Du LL, Limbo O, Williams JS, Russell P. BRCT domain interactions with phospho-histone H2A target Crb2 to chromatin at double-strand breaks and maintain the DNA damage checkpoint. Mol Cell Biol. 2010;30(19):4732-43. Epub 2010/08/04. doi: 10.1128/MCB.00413-10. PubMed PMID: 20679485; PubMed Central PMCID: PMCPMC2950532.
19. Wei Y, Wang HT, Zhai Y, Russell P, Du LL. Mdb1, a fission yeast homolog of human MDC1, modulates DNA damage response and mitotic spindle function. PLoS One. 2014;9(5):e97028. Epub 2014/05/09. doi: 10.1371/journal.pone.0097028. PubMed PMID: 24806815; PubMed Central PMCID: PMCPMC4013092.
20. Roitinger E, Hofer M, Kocher T, Pichler P, Novatchkova M, Yang J, et al. Quantitative phosphoproteomics of the ataxia telangiectasia-mutated (ATM) and ataxia telangiectasia-mutated and rad3-related (ATR) dependent DNA damage response in Arabidopsis thaliana. Mol Cell Proteomics. 2015;14(3):556-71. Epub 2015/01/07. doi: 10.1074/mcp.M114.040352

M114.040352 [pii]. PubMed PMID: 25561503; PubMed Central PMCID: PMC4349977.

21. Yelagandula R, Stroud H, Holec S, Zhou K, Feng S, Zhong X, et al. The histone variant H2A.W defines heterochromatin and promotes chromatin condensation in Arabidopsis. Cell. 2014;158(1):98-109. Epub 2014/07/06. doi: 10.1016/j.cell.2014.06.006

S0092-8674(14)00727-2 [pii]. PubMed PMID: 24995981; PubMed Central PMCID: PMC4671829.

22. Osakabe A, Lorkovic ZJ, Kobayashi W, Tachiwana H, Yelagandula R, Kurumizaka H, et al. Histone H2A variants confer specific properties to nucleosomes and impact on chromatin accessibility. Nucleic Acids Res. 2018;46(15):7675-85. doi: 10.1093/nar/gky540. PubMed PMID: 29945241; PubMed Central PMCID: PMCPMC6125630.

23. Kawashima T, Lorkovic ZJ, Nishihama R, Ishizaki K, Axelsson E, Yelagandula R, et al. Diversification of histone H2A variants during plant evolution. Trends Plant Sci. 2015;20(7):419-25. Epub 2015/05/20. doi: 10.1016/j.tplants.2015.04.005. PubMed PMID: 25983206.

24. Li Z, Kono H. Distinct Roles of Histone H3 and H2A Tails in Nucleosome Stability. Sci Rep. 2016;6:31437. doi: 10.1038/srep31437. PubMed PMID: 27527579; PubMed Central PMCID: PMCPMC4985630.

25. Lei B, Capella M, Montgomery SA, Borg M, Osakabe A, Goiser M, et al. A Synthetic Approach to Reconstruct the Evolutionary and Functional Innovations of the Plant Histone Variant H2A.W. Curr Biol. 2020. Epub 2020/10/24. doi: 10.1016/j.cub.2020.09.080. PubMed PMID: 33096036.

26. Douet J, Corujo D, Malinverni R, Renauld J, Sansoni V, Posavec Marjanovic M, et al. MacroH2A histone variants maintain nuclear organization and heterochromatin architecture. J Cell Sci. 2017;130(9):1570-82. doi: 10.1242/jcs.199216. PubMed PMID: 28283545.

27. Fyodorov DV, Zhou BR, Skoultchi AI, Bai Y. Emerging roles of linker histones in regulating chromatin structure and function. Nat Rev Mol Cell Biol. 2018;19(3):192-206. doi: 10.1038/nrm.2017.94. PubMed PMID: 29018282; PubMed Central PMCID: PMCPMC5897046.

28. Kozlowski M, Corujo D, Hothorn M, Guberovic I, Mandemaker IK, Blessing C, et al. MacroH2A histone variants limit chromatin plasticity through two distinct mechanisms. EMBO Rep. 2018;19(10). doi: 10.15252/embr.201744445. PubMed PMID: 30177554; PubMed Central PMCID: PMCPMC6172464.

29. Roque A, Ponte I, Arrondo JL, Suau P. Phosphorylation of the carboxy-terminal domain of histone H1: effects on secondary structure and DNA condensation. Nucleic Acids Res. 2008;36(14):4719-26. doi: 10.1093/nar/gkn440. PubMed PMID: 18632762; PubMed Central PMCID: PMCPMC2504289.

30. Izzo A, Schneider R. The role of linker histone H1 modifications in the regulation of gene expression and chromatin dynamics. Biochim Biophys Acta. 2016;1859(3):486-95. doi: 10.1016/j.bbagrm.2015.09.003. PubMed PMID: 26348411.

31. Kotlinski M, Rutowicz K, Knizewski L, Palusinski A, Oledzki J, Fogtman A, et al. Histone H1 Variants in Arabidopsis Are Subject to Numerous Post-Translational Modifications, Both Conserved and Previously Unknown in Histones, Suggesting Complex Functions of H1 in Plants. PLoS One. 2016;11(1):e0147908. doi: 10.1371/journal.pone.0147908. PubMed PMID: 26820416; PubMed Central PMCID: PMCPMC4731575.

32. Ausio J, Van Holde KE. The histones of the sperm of Spisula solidissima include a novel, cysteine-containing H-1 histone. Cell Differ. 1988;23(3):175-89. Epub 1988/04/01. doi: 10.1016/0045-6039(88)90070-x. PubMed PMID: 3378268.

33. Bonisch C, Hake SB. Histone H2A variants in nucleosomes and chromatin: more or less stable? Nucleic Acids Res. 2012;40(21):10719-41. Epub 2012/09/25. doi: 10.1093/nar/gks865. PubMed PMID: 23002134; PubMed Central PMCID: PMCPMC3510494.

34. Molaro A, Young JM, Malik HS. Evolutionary origins and diversification of testis-specific short histone H2A variants in mammals. Genome Res. 2018;28(4):460-73. doi: 10.1101/gr.229799.117. PubMed PMID: 29549088; PubMed Central PMCID: PMCPMC5880237.

35. Lei B, Berger F. H2A Variants in Arabidopsis: Versatile Regulators of Genome Activity. Plant Communications. 2020;1(1). doi: https://doi.org/10.1016/j.xplc.2019.100015.

36. Baldi S, Becker PB. The variant histone H2A.V of Drosophila--three roles, two guises. Chromosoma. 2013;122(4):245-58. Epub 2013/04/05. doi: 10.1007/s00412-013-0409-x. PubMed PMID: 23553272.

831 37. Dantuma NP, van Attikum H. Spatiotemporal regulation of posttranslational modifications in
832 the DNA damage response. EMBO J. 2016;35(1):6-23. Epub 2015/12/03. doi:
833 10.15252/embj.201592595

834 embj.201592595 [pii]. PubMed PMID: 26628622; PubMed Central PMCID: PMC4717999.
835 38. Talbert PB, Henikoff S. Environmental responses mediated by histone variants. Trends Cell
836 Biol. 2014;24(11):642-50. Epub 2014/08/26. doi: 10.1016/j.tcb.2014.07.006

837 S0962-8924(14)00120-2 [pii]. PubMed PMID: 25150594.
838 39. Muller S, Almouzni G. Chromatin dynamics during the cell cycle at centromeres. Nat Rev
839 Genet. 2017;18(3):192-208. doi: 10.1038/nrg.2016.157. PubMed PMID: 28138144.
840 40. Jacob Y, Bergamin E, Donoghue MT, Mongeon V, LeBlanc C, Voigt P, et al. Selective
841 methylation of histone H3 variant H3.1 regulates heterochromatin replication. Science.
842 2014;343(6176):1249-53. doi: 10.1126/science.1248357. PubMed PMID: 24626927; PubMed Central
843 PMCID: PMCPMC4049228.
844 41. Borg M, Jacob Y, Susaki D, LeBlanc C, Buendia D, Axelsson E, et al. Targeted reprogramming
845 of H3K27me3 resets epigenetic memory in plant paternal chromatin. Nat Cell Biol. 2020;22(6):621-9.
846 Epub 2020/05/13. doi: 10.1038/s41556-020-0515-y. PubMed PMID: 32393884.
847 42. Yan A, Borg M, Berger F, Chen Z. The atypical histone variant H3.15 promotes callus formation
848 in Arabidopsis thaliana. Development. 2020;147(11). Epub 2020/05/23. doi: 10.1242/dev.184895.
849 PubMed PMID: 32439757.
850 43. Giaimo BD, Ferrante F, Herchenrother A, Hake SB, Borggrefe T. The histone variant H2A.Z in
851 gene regulation. Epigenetics Chromatin. 2019;12(1):37. doi: 10.1186/s13072-019-0274-9. PubMed
852 PMID: 31200754; PubMed Central PMCID: PMCPMC6570943.
853 44. Zhang K, Sridhar VV, Zhu J, Kapoor A, Zhu JK. Distinctive core histone post-translational
854 modification patterns in Arabidopsis thaliana. PLoS One. 2007;2(11):e1210. doi:
855 10.1371/journal.pone.0001210. PubMed PMID: 18030344; PubMed Central PMCID:
856 PMCPMC2075165.
857 45. Shaltiel IA, Krenning L, Bruinsma W, Medema RH. The same, only different - DNA damage
858 checkpoints and their reversal throughout the cell cycle. J Cell Sci. 2015;128(4):607-20. doi:
859 10.1242/jcs.163766. PubMed PMID: 25609713.
860 46. Lanz MC, Dibitetto D, Smolka MB. DNA damage kinase signaling: checkpoint and repair at 30
861 years. EMBO J. 2019;38(18):e101801. doi: 10.15252/embj.2019101801. PubMed PMID: 31393028;
862 PubMed Central PMCID: PMCPMC6745504.
863 47. Meijer L, Borgne A, Mulner O, Chong JP, Blow JJ, Inagaki N, et al. Biochemical and cellular
864 effects of roscovitine, a potent and selective inhibitor of the cyclin-dependent kinases cdc2, cdk2 and
865 cdk5. Eur J Biochem. 1997;243(1-2):527-36. PubMed PMID: 9030781.
866 48. Joubes J, Chevalier C, Dudits D, Heberle-Bors E, Inze D, Umeda M, et al. CDK-related protein
867 kinases in plants. Plant Mol Biol. 2000;43(5-6):607-20. PubMed PMID: 11089864.
868 49. Francis D. The plant cell cycle--15 years on. New Phytol. 2007;174(2):261-78. doi:
869 10.1111/j.1469-8137.2007.02038.x. PubMed PMID: 17388890.
870 50. Nowack MK, Harashima H, Dissmeyer N, Zhao X, Bouyer D, Weimer AK, et al. Genetic
871 framework of cyclin-dependent kinase function in Arabidopsis. Dev Cell. 2012;22(5):1030-40. doi:
872 10.1016/j.devcel.2012.02.015. PubMed PMID: 22595674.
873 51. Dissmeyer N, Nowack MK, Pusch S, Stals H, Inze D, Grini PE, et al. T-loop phosphorylation
874 of Arabidopsis CDKA;1 is required for its function and can be partially substituted by an aspartate
875 residue. Plant Cell. 2007;19(3):972-85. doi: 10.1105/tpc.107.050401. PubMed PMID: 17369369;
876 PubMed Central PMCID: PMCPMC1867360.
877 52. Dissmeyer N, Weimer AK, Pusch S, De Schutter K, Alvim Kamei CL, Nowack MK, et al.
878 Control of cell proliferation, organ growth, and DNA damage response operate independently of
879 dephosphorylation of the Arabidopsis Cdk1 homolog CDKA;1. Plant Cell. 2009;21(11):3641-54. doi:
880 10.1105/tpc.109.070417. PubMed PMID: 19948791; PubMed Central PMCID: PMCPMC2798325.
881 53. Porceddu A, Stals H, Reichheld JP, Segers G, De Veylder L, Barroco RP, et al. A plant-specific
882 cyclin-dependent kinase is involved in the control of G2/M progression in plants. J Biol Chem.
883 2001;276(39):36354-60. doi: 10.1074/jbc.M011060200. PubMed PMID: 11477067.

884 54. Carr AM, Dorrington SM, Hindley J, Phear GA, Aves SJ, Nurse P. Analysis of a histone H2A
885 variant from fission yeast: evidence for a role in chromosome stability. Mol Gen Genet.
886 1994;245(5):628-35. PubMed PMID: 7808414.
887 55. Choe J, Schuster T, Grunstein M. Organization, primary structure, and evolution of histone H2A
888 and H2B genes of the fission yeast Schizosaccharomyces pombe. Mol Cell Biol. 1985;5(11):3261-9.
889 doi: 10.1128/mcb.5.11.3261. PubMed PMID: 3018512; PubMed Central PMCID: PMCPMC369142.
890 56. Su Y, Wang S, Zhang F, Zheng H, Liu Y, Huang T, et al. Phosphorylation of Histone H2A at
891 Serine 95: A Plant-Specific Mark Involved in Flowering Time Regulation and H2A.Z Deposition. Plant
892 Cell. 2017;29(9):2197-213. doi: 10.1105/tpc.17.00266. PubMed PMID: 28790150; PubMed Central
893 PMCID: PMCPMC5635989.
894 57. Dong Q, Han F. Phosphorylation of histone H2A is associated with centromere function and
895 maintenance in meiosis. Plant J. 2012;71(5):800-9. doi: 10.1111/j.1365-313X.2012.05029.x. PubMed
896 PMID: 22519817.
897 58. Su H, Liu Y, Dong Q, Feng C, Zhang J, Liu Y, et al. Dynamic location changes of Bub1-
898 phosphorylated-H2AThr133 with CENH3 nucleosome in maize centromeric regions. New Phytol.
899 2017;214(2):682-94. doi: 10.1111/nph.14415. PubMed PMID: 28079247.
900 59. Yamagishi Y, Honda T, Tanno Y, Watanabe Y. Two histone marks establish the inner
901 centromere and chromosome bi-orientation. Science. 2010;330(6001):239-43. doi:
902 10.1126/science.1194498. PubMed PMID: 20929775.
903 60. Wang F, Higgins JM. Histone modifications and mitosis: countermarks, landmarks, and
904 bookmarks. Trends Cell Biol. 2013;23(4):175-84. Epub 2012/12/19. doi: 10.1016/j.tcb.2012.11.005
905 S0962-8924(12)00219-X [pii]. PubMed PMID: 23246430.
906 61. Aihara H, Nakagawa T, Mizusaki H, Yoneda M, Kato M, Doiguchi M, et al. Histone H2A T120
907 Phosphorylation Promotes Oncogenic Transformation via Upregulation of Cyclin D1. Mol Cell.
908 2016;64(1):176-88. doi: 10.1016/j.molcel.2016.09.012. PubMed PMID: 27716482.
909 62. Maeda K, Yoneda M, Nakagawa T, Ikeda K, Higashi M, Nakagawa K, et al. Defects in
910 centromeric/pericentromeric histone H2A T120 phosphorylation by hBUB1 cause chromosome
911 missegregation producing multinucleated cells. Genes Cells. 2018;23(10):828-38. doi:
912 10.1111/gtc.12630. PubMed PMID: 30112853.
913 63. Wang H, Wang L, Erdjument-Bromage H, Vidal M, Tempst P, Jones RS, et al. Role of histone
914 H2A ubiquitination in Polycomb silencing. Nature. 2004;431(7010):873-8. doi: 10.1038/nature02985.
915 PubMed PMID: 15386022.
916 64. Nakagawa T, Kajitani T, Togo S, Masuko N, Ohdan H, Hishikawa Y, et al. Deubiquitylation of
917 histone H2A activates transcriptional initiation via trans-histone cross-talk with H3K4 di- and
918 trimethylation. Genes Dev. 2008;22(1):37-49. doi: 10.1101/gad.1609708. PubMed PMID: 18172164;
919 PubMed Central PMCID: PMCPMC2151013.
920 65. Zhou W, Zhu P, Wang J, Pascual G, Ohgi KA, Lozach J, et al. Histone H2A monoubiquitination
921 represses transcription by inhibiting RNA polymerase II transcriptional elongation. Mol Cell.
922 2008;29(1):69-80. doi: 10.1016/j.molcel.2007.11.002. PubMed PMID: 18206970; PubMed Central
923 PMCID: PMCPMC2327256.
924 66. Chu F, Nusinow DA, Chalkley RJ, Plath K, Panning B, Burlingame AL. Mapping post-
925 translational modifications of the histone variant MacroH2A1 using tandem mass spectrometry. Mol
926 Cell Proteomics. 2006;5(1):194-203. doi: 10.1074/mcp.M500285-MCP200. PubMed PMID: 16210244.
927 67. Ku M, Jaffe JD, Koche RP, Rheinbay E, Endoh M, Koseki H, et al. H2A.Z landscapes and dual
928 modifications in pluripotent and multipotent stem cells underlie complex genome regulatory functions.
929 Genome Biol. 2012;13(10):R85. doi: 10.1186/gb-2012-13-10-r85. PubMed PMID: 23034477; PubMed
930 Central PMCID: PMCPMC3491413.
931 68. Ogawa Y, Ono T, Wakata Y, Okawa K, Tagami H, Shibahara KI. Histone variant macroH2A1.2
932 is mono-ubiquitinated at its histone domain. Biochem Biophys Res Commun. 2005;336(1):204-9. doi:
933 10.1016/j.bbrc.2005.08.046. PubMed PMID: 16129414.
934 69. Pan MR, Peng G, Hung WC, Lin SY. Monoubiquitination of H2AX protein regulates DNA
935 damage response signaling. J Biol Chem. 2011;286(32):28599-607. doi: 10.1074/jbc.M111.256297.
936 PubMed PMID: 21676867; PubMed Central PMCID: PMCPMC3151101.
937 70. Sarcinella E, Zuzarte PC, Lau PN, Draker R, Cheung P. Monoubiquitylation of H2A.Z
938 distinguishes its association with euchromatin or facultative heterochromatin. Mol Cell Biol.

939 2007;27(18):6457-68. doi: 10.1128/MCB.00241-07. PubMed PMID: 17636032; PubMed Central
940 PMCID: PMCPMC2099601.
941 71. Schwertman P, Bekker-Jensen S, Mailand N. Regulation of DNA double-strand break repair by
942 ubiquitin and ubiquitin-like modifiers. Nat Rev Mol Cell Biol. 2016;17(6):379-94. doi:
943 10.1038/nrm.2016.58. PubMed PMID: 27211488.
944 72. Wu CY, Kang HY, Yang WL, Wu J, Jeong YS, Wang J, et al. Critical role of
945 monoubiquitination of histone H2AX protein in histone H2AX phosphorylation and DNA damage
946 response. J Biol Chem. 2011;286(35):30806-15. doi: 10.1074/jbc.M111.257469. PubMed PMID:
947 21690091; PubMed Central PMCID: PMCPMC3162441.
948 73. Nowack MK, Shirzadi R, Dissmeyer N, Dolf A, Endl E, Grini PE, et al. Bypassing genomic
949 imprinting allows seed development. Nature. 2007;447(7142):312-5. doi: 10.1038/nature05770.
950 PubMed PMID: 17468744.
951 74. Lampropoulos A, Sutikovic Z, Wenzl C, Maegele I, Lohmann JU, Forner J. GreenGate---a
952 novel, versatile, and efficient cloning system for plant transgenesis. PLoS One. 2013;8(12):e83043.
953 Epub 2014/01/01. doi: 10.1371/journal.pone.0083043. PubMed PMID: 24376629; PubMed Central
954 PMCID: PMCPMC3869738.
955 75. Taus T, Kocher T, Pichler P, Paschke C, Schmidt A, Henrich C, et al. Universal and confident
956 phosphorylation site localization using phosphoRS. J Proteome Res. 2011;10(12):5354-62. doi:
957 10.1021/pr200611n. PubMed PMID: 22073976.
958 76. Kumagai-Sano F, Hayashi T, Sano T, Hasezawa S. Cell cycle synchronization of tobacco BY-
959 2 cells. Nat Protoc. 2006;1(6):2621-7. doi: 10.1038/nprot.2006.381. PubMed PMID: 17406517.
960 77. Sauer M, Paciorek T, Benkova E, Friml J. Immunocytochemical techniques for whole-mount in
961 situ protein localization in plants. Nat Protoc. 2006;1(1):98-103. doi: 10.1038/nprot.2006.15. PubMed
962 PMID: 17406218.
963 78. Lorkovic ZJ, Hilscher J, Barta A. Use of fluorescent protein tags to study nuclear organization
964 of the spliceosomal machinery in transiently transformed living plant cells. Mol Biol Cell.
965 2004;15(7):3233-43. Epub 2004/05/11. doi: 10.1091/mbc.E04-01-0055

966 E04-01-0055 [pii]. PubMed PMID: 15133128; PubMed Central PMCID: PMC452579.
967 79. Tachiwana H, Kagawa W, Osakabe A, Kawaguchi K, Shiga T, Hayashi-Takanaka Y, et al.
968 Structural basis of instability of the nucleosome containing a testis-specific histone variant, human H3T.
969 Proc Natl Acad Sci U S A. 2010;107(23):10454-9. doi: 10.1073/pnas.1003064107. PubMed PMID:
970 20498094; PubMed Central PMCID: PMCPMC2890842.
971 80. Tanaka Y, Tawaramoto-Sasanuma M, Kawaguchi S, Ohta T, Yoda K, Kurumizaka H, et al.
972 Expression and purification of recombinant human histones. Methods. 2004;33(1):3-11. doi:
973 10.1016/j.ymeth.2003.10.024. PubMed PMID: 15039081.
974 81. Gregan J, Rabitsch PK, Rumpf C, Novatchkova M, Schleiffer A, Nasmyth K. High-throughput
975 knockout screen in fission yeast. Nat Protoc. 2006;1(5):2457-64. doi: 10.1038/nprot.2006.385. PubMed
976 PMID: 17406492; PubMed Central PMCID: PMCPMC2957175.
977 82. Kunoh T, Habu T. Pcf1, a large subunit of CAF-1, required for maintenance of checkpoint
978 kinase Cds1 activity. Springerplus. 2014;3:30. doi: 10.1186/2193-1801-3-30. PubMed PMID:
979 24478943; PubMed Central PMCID: PMCPMC3902073.
980 83. Pidoux A, Mellone B, Allshire R. Analysis of chromatin in fission yeast. Methods.
981 2004;33(3):252-9. doi: 10.1016/j.ymeth.2003.11.021. PubMed PMID: 15157893.
982 84. Roguev A, Wiren M, Weissman JS, Krogan NJ. High-throughput genetic interaction mapping
983 in the fission yeast Schizosaccharomyces pombe. Nat Methods. 2007;4(10):861-6. Epub 2007/09/26.
984 doi: 10.1038/nmeth1098. PubMed PMID: 17893680.
985 85. Dixon SJ, Fedyshyn Y, Koh JL, Prasad TS, Chahwan C, Chua G, et al. Significant conservation
986 of synthetic lethal genetic interaction networks between distantly related eukaryotes. Proc Natl Acad Sci
987 U S A. 2008;105(43):16653-8. Epub 2008/10/22. doi: 10.1073/pnas.0806261105. PubMed PMID:
988 18931302; PubMed Central PMCID: PMCPMC2575475.
989 86. Barrales RR, Forn M, Georgescu PR, Sarkadi Z, Braun S. Control of heterochromatin
990 localization and silencing by the nuclear membrane protein Lem2. Genes Dev. 2016;30(2):133-48. Epub
991 2016/01/09. doi: 10.1101/gad.271288.115. PubMed PMID: 26744419; PubMed Central PMCID:
992 PMCPMC4719305.

993 **Figure and legends**

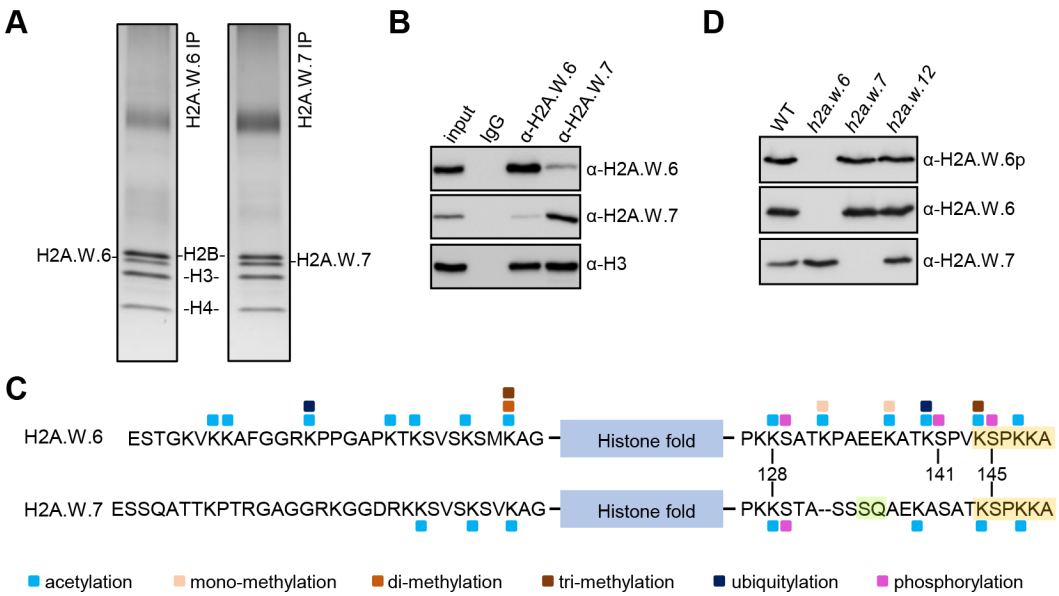

994

995 **Fig 1. H2A.W.6 and H2A.W.7 carry distinct PTMs.** (A) Silver stained gels of H2A.W.6 and
996 H2A.W.7 mononucleosomes immunoprecipitated from MNase digested nuclear extracts from
997 leaves. Bands corresponding to H2A.W.6 and H2A.W.7 were excised and analyzed by mass
998 spectrometry (MS). (B) Western blot analysis of immunoprecipitates obtained with H2A.W.6
999 and H2A.W.7 specific antibodies from MNase digested WT nuclei. Note that H2A.W.6 and
1000 H2A.W.7 nucleosomes contain small amounts of H2A.W.7 and H2A.W.6, respectively, as
1001 previously reported [16, 22]. (C) Summary of all PTMs detected on H2A.W.6 and H2A.W.7.
1002 Amino acid sequence of N- and C-terminal tails of H2A.W.6 and H2A.W.7 are indicated with
1003 the conserved H2A.W KSPK motif and H2A.W.7 SQ motif highlighted in orange and green,
1004 respectively. The blue box indicates the histone fold domain. Post-translational modifications
1005 detected by MS are color-coded as indicated at the bottom. (D) Western blot analysis of nuclear
1006 extract from twelve days old WT, *hta6*, *hta7,* and *hta12* mutant seedlings with antibodies
1007 against H2A.W.6p, H2A.W.6, and H2A.W.7.

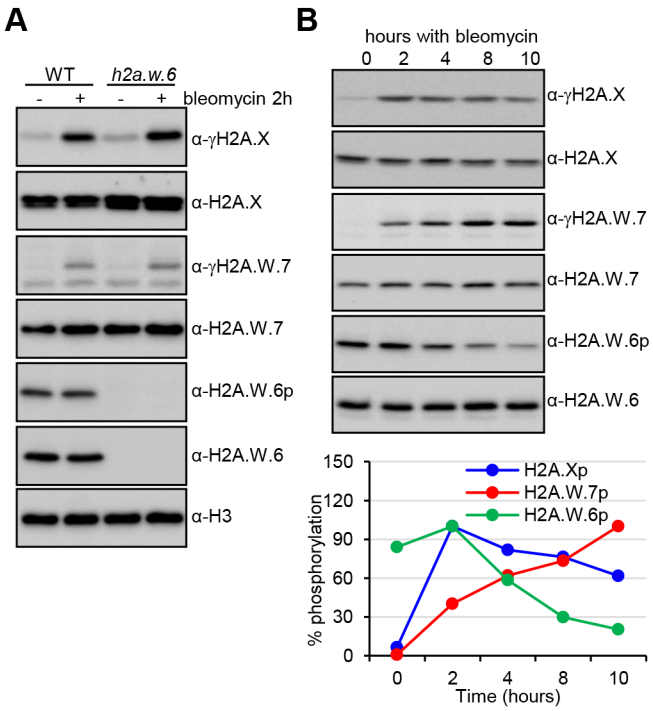

1008

1009 **Fig 2. Phosphorylation of the H2A.W KSPK motif is not induced by DNA damage.** (A)
1010 Phosphorylation of the KSPK motif on H2A.W.7 cannot be triggered by DNA damage. WT
1011 and *hta6* mutant seedlings were either mock or bleomycin (20 µg/ml) treated for two hours and
1012 nuclear extracts were analyzed by western blotting with indicated antibodies. (B) *Arabidopsis*
1013 WT seedlings were treated with 20 µg/ml of bleomycin for the indicated time periods and
1014 protein extracts were analyzed with the indicated antibodies. Levels of γH2A.X, γH2A.W.7,
1015 and H2A.W.6p (bottom panel) were quantified by normalization to the total level of the
1016 respective variant at each time point.

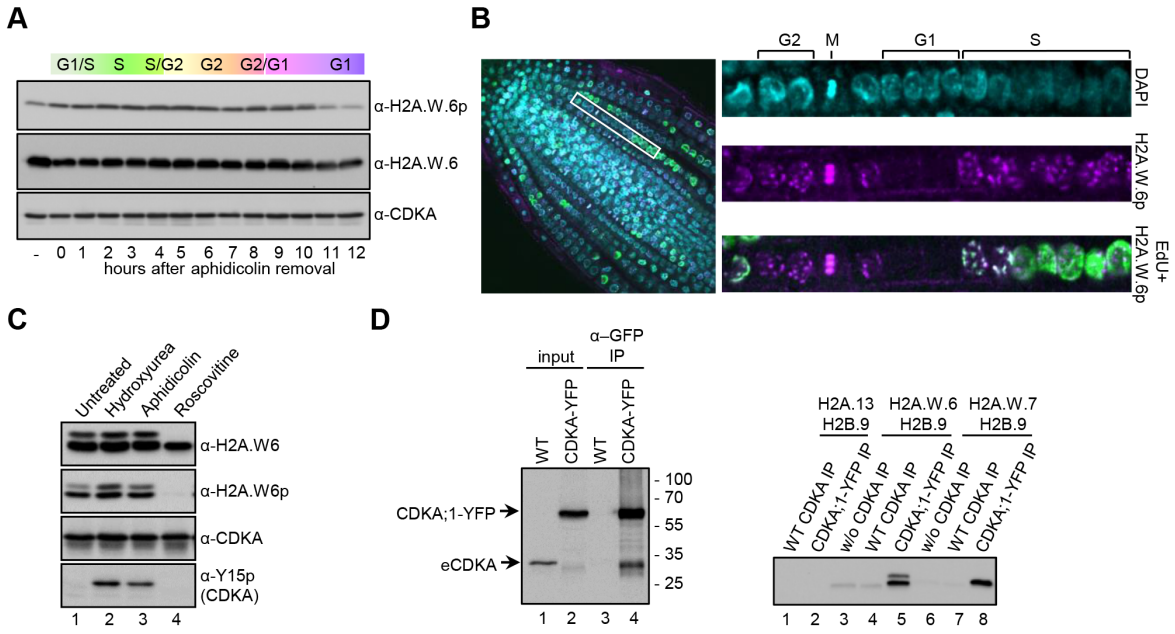

Fig 3. H2A.W.6 is phosphorylated in a cell cycle dependent manner by cyclin dependent protein kinases (CDK). (A) Phosphorylation of the KSPK motif is cell cycle dependent in tobacco BY-2 cell suspension culture. BY-2 cells were synchronized with 20 µg/ml aphidicolin for 24 hours. Protein extracts from samples taken in one-hour intervals after release of the block were analyzed by western blotting with the indicated antibodies. (B) Confocal images of WT root tips immunostained with H2A.W.6p antibody (magenta) after EdU (green) incorporation. Enlarged images of a row of cells in different cell cycle stages (indicated on the top) are shown on the right. (C) Protein extracts from *Arabidopsis* cell suspension treated with cell cycle inhibitors were analyzed by western blotting with the indicated antibodies. Inhibitory phosphorylation of CDK at tyrosine 15 (Y15) upon hydroxyurea and aphidicolin treatment (bottom panel, lanes 2 and 3) demonstrate the specificity and robustness of the assay. By contrast, roscovitine that inhibits the CDK activity directly by binding to the ATP binding pocket does not induce Y15 phosphorylation. (D) *Arabidopsis* CDKA;1-YFP was immunoprecipitated from whole cell extracts and detected with an anti-CDK antibody (left panel, lanes 2 and 4) and used in an *in vitro* kinase assay (right panel) with recombinant histone H2A-H2B dimers as indicated. Phosphorylation of the KSPKK motif was detected by western blotting with H2A.W.6p antibody. Note that GFP beads do not precipitate wild-type CDKA;1 (left panel, lane 3) and consequently H2A.W.6p was not detected in kinase assays from these IPs (right panel, lanes 4 and 7).

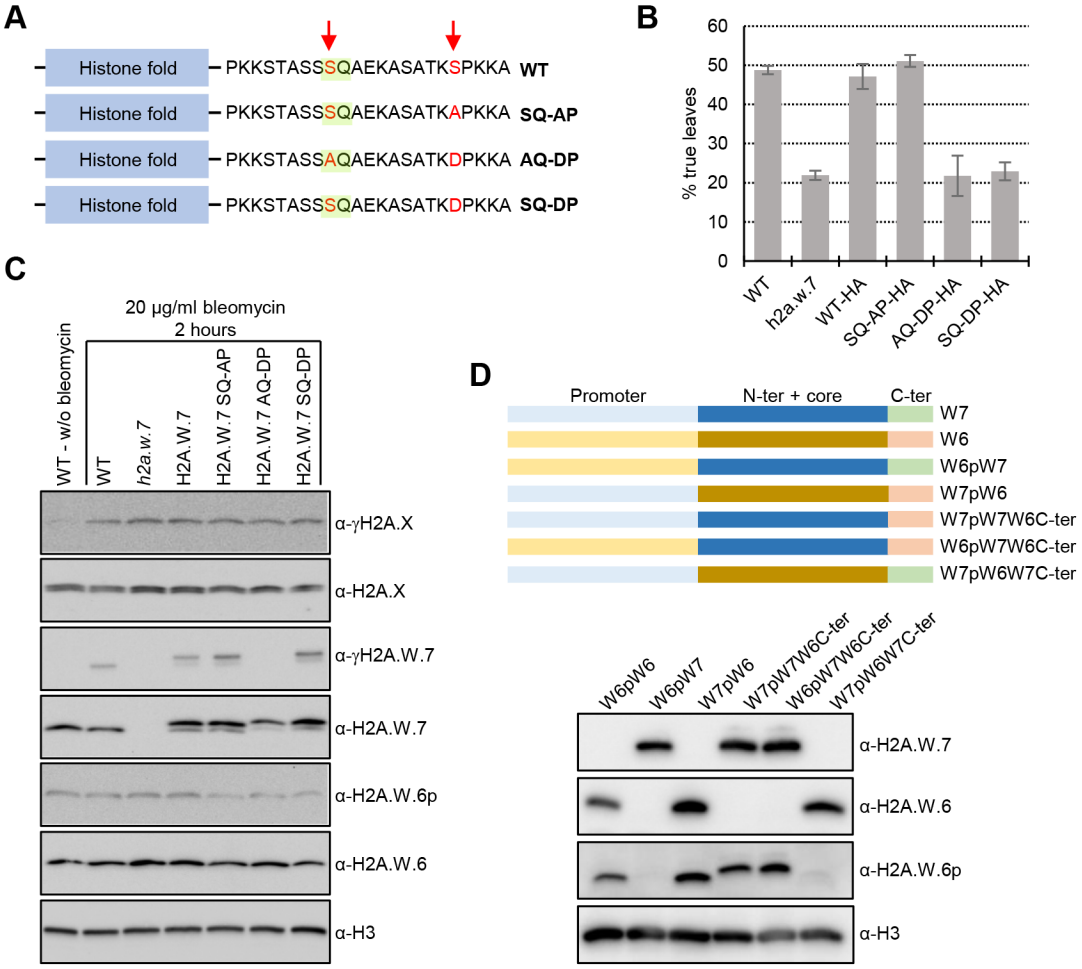

1038

1039 **Fig 4. Phosphomimic of KSPK phosphorylation results in DNA damage sensitivity *in***
1040 ***planta*.** (A) Schematic diagrams of *Arabidopsis* H2A.W.7 variants containing mutated serin
1041 residues (in red) in the SQ (highlighted in green) and KSPK motifs. (B) Phosphomimic of the
1042 KSPK motif confers DNA damage sensitivity. Seeds from *h2a.w.7* mutants expressing HA-
1043 tagged WT H2A.W.7 or H2A.W.7 with mutations in the SQ and KSPK motifs were germinated
1044 in the presence of 50 mg/mL of zeocin and scored for true leaf development twelve days after
1045 germination. Data are represented as means ±SD of three independent experiments with n>400
1046 seedlings. (C) Phosphomimic of the KSPK motif does not prevent SQ motif phosphorylation
1047 of H2A.W.7. Seedlings grown for 10 days on MS plates were treated for two hours with 20
1048 µg/ml of bleomycin and nuclear extracts were analyzed by western blotting with the indicated
1049 antibodies. (D) Primary sequence of the H2A.W C-terminal tail determines phosphorylation
1050 outcome of the KSPK motif. Schemes of promoter, histone core domain and C-terminal tail
1051 swaps between H2A.W.6 and H2A.W.7 (top panel). Western blot analysis of expression and
1052 KSPK motif phosphorylation of nuclear extracts from plants expressing indicated H2A.W swap
1053 versions in mutant plants deprived from H2A.W (bottom panel).
1054

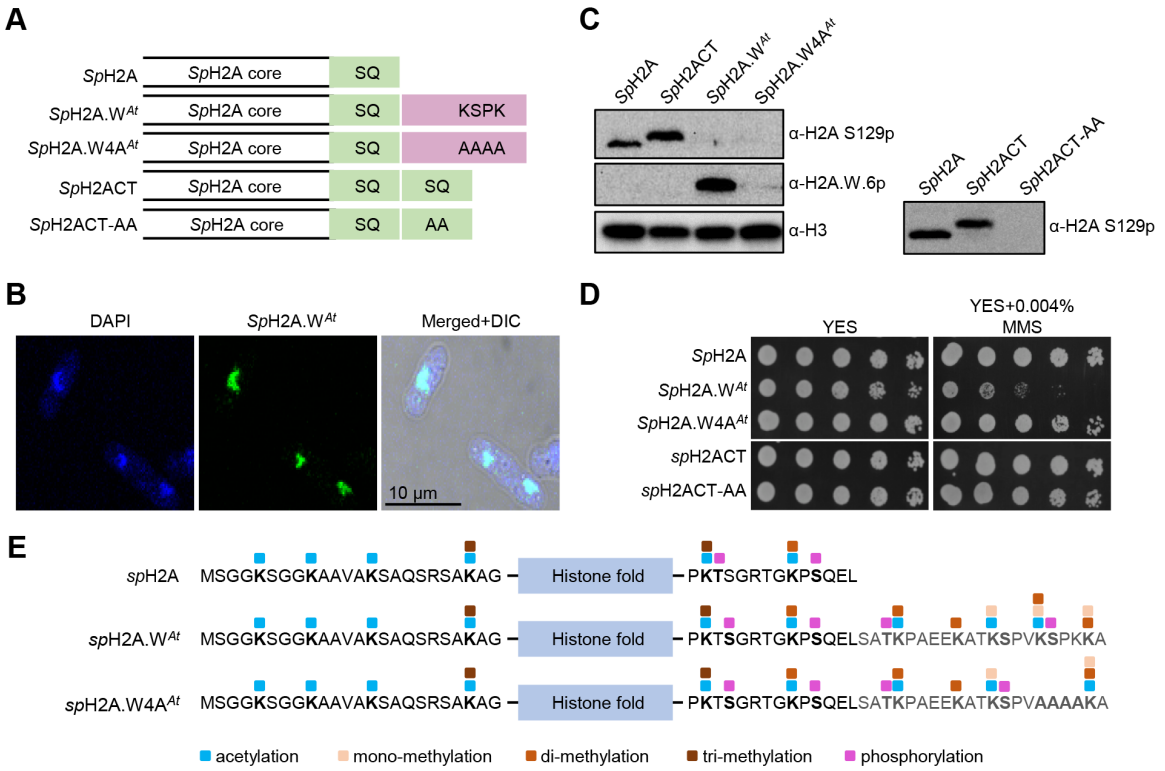

Fig 5. Phosphorylation of the KSPK motifs results in DNA damage sensitivity in yeast. (A) Schematic diagrams of fission yeast histone H2A (*Sp*H2A) and mosaic versions containing either a duplicated C-terminal tail (*Sp*H2ACT) or the C-terminal tail from *Arabidopsis* H2A.W.6 (*Sp*H2A.W^{At}). Mutant versions in the SQ and KSPK motifs of the latter two constructs, *Sp*H2ACT-AA and *Sp*H2A.W4A^{At}, are also depicted. (B) *Sp*H2A.W^{At} localizes to the nucleus in fission yeast. Confocal images of immunostained cells from exponential phase are shown. 4′,6-diamidino-2-phenylindole (DAPI) staining was used to visualize nuclei and differential interference contrast (DIC) for cell shape. (C) Analysis of *Sp*H2A S129 (SQ) and of *Sp*H2A.W^{At} (KSPK) phosphorylation in indicated yeast strains. Cells were collected during exponential growth and whole cell extracts were analyzed with the indicated antibodies, using anti-histone H3 antibody as loading control. The lack of SQ phosphorylation signal in strains expressing *Sp*H2A.W^{At}, *Sp*H2A.W4A^{At}, and *Sp*H2ACT-AA is due to the inability of the antibody to bind to the epitope. Phosphorylation of the SQ motif in these strains was confirmed by mass spectrometry (S5D Fig). (D) Phosphorylation of *Sp*H2A.W^{At} at the KSPK motif confers sensitivity to DNA damage. Serial dilutions of fission yeast cells expressing WT and indicated *Sp*H2A mosaic variants were spotted onto either YES or YES plates containing 0.004% methyl methane sulfonate (MMS) and incubated at 32°C for 3 days. (E) Summary of all PTMs detected on *Sp*H2A in WT and chimeric histone in indicated yeast strains. Amino acid sequence of N- and C-terminal tails of chimeric histone are indicated with the conserved *Sp*H2A SQ motif and H2A.W.6 KSPK motif respectively. The blue box indicates the histone fold domain. Post-translational modifications detected by MS are color-coded as indicated at the bottom.

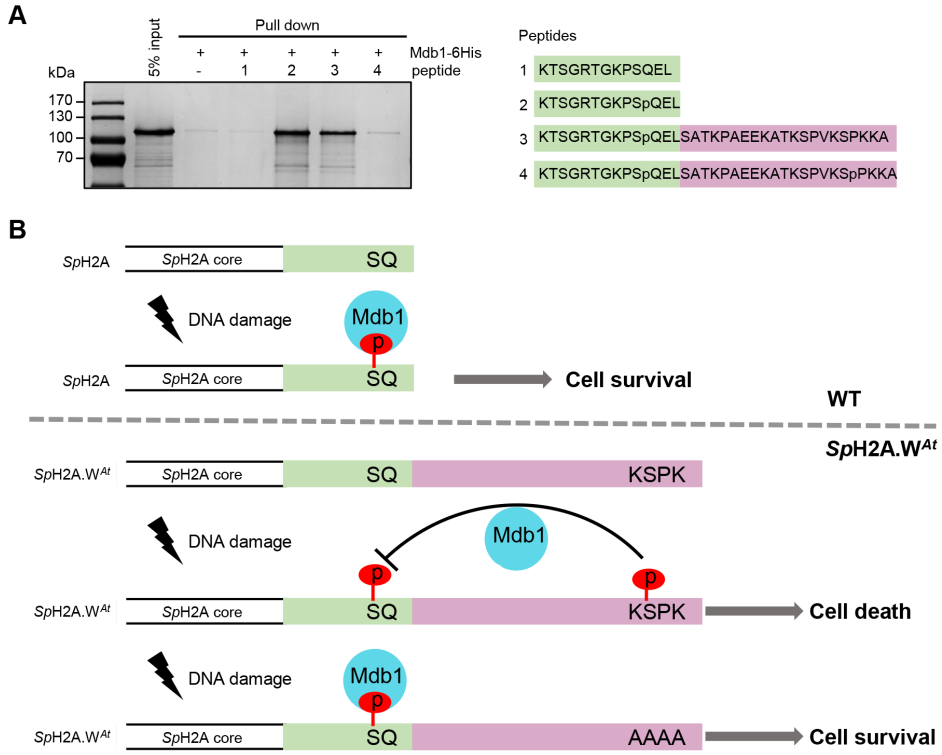

1078

1079 **Fig 6. KSPK motif directly interferes with binding of Mdb1 to phosphorylated SQ in a**
1080 **phosphorylation dependent manner.** (A) Mdb1 recombinant protein was expressed in *E. coli*
1081 BL21 and purified using Ni-NTA beads. Biotinylated peptides, as depicted on the right,
1082 corresponding to C terminus of *Sp*H2A, with unmodified (SQ) or S129 phosphorylation (SpQ),
1083 or SpQ with unmodified KSPK motif (SpQ+KSPK) or SpQ with S145 phosphorylation
1084 (SpQ+KSpPK), were incubated with streptavidin Dynabeads and Mdb1 recombinant protein.
1085 The eluates were analyzed by SDS-PAGE with Coomassie staining. (B) The model of crosstalk
1086 between SQ and KSPK phosphorylation. In WT cell, S129 phosphorylation site recruit Mdb1
1087 as platform for downstream DDR in response to DNA damage. In *Sp*H2A.W^{At} cell, KSPK
1088 phosphorylation prevents the Mdb1 binding to SQ phosphorylation site, thus DNA cannot
1089 repair properly. In *Sp*H2A.W4A^{At} cell, the absence of KSPK phosphorylation allowed the
1090 Mdb1 binding to phosphorylated SQ to recruit DDR for DNA repair.

1091

1092 **Supplemental Figures**

1093

1094 **S1 Fig. Mass spectrometry analysis of H2A.W.6 and H2A.W.7 modifications.** Summary of

1095 all modifications detected with samples from leaves, flowers, and seedlings.

1096

1097

1098

1099

1100

1101

1102

1103

1104

1105

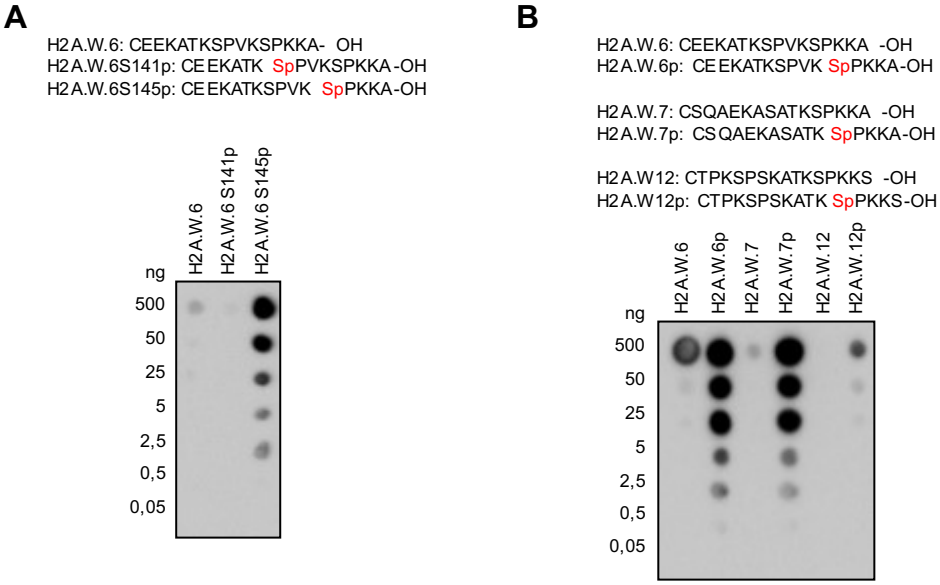

1106

1107 **S2 Fig. Antibody against the phosphorylated serine 145 of H2A.W.6 is specific but**
1108 **recognizes the phosphorylated KSPKKA motif of H2A.W.7.** (**A**) Affinity purified antibody
1109 obtained after immunization of rabbits with the CEEKATKSPVKSpPKKA-OH peptide were
1110 tested on dot blots with the serially diluted peptides indicated at the top. Note that
1111 unphosphorylated peptide or peptide phosphorylated at serine 141 do not cross-react with the
1112 affinity purified antibody. (**B**) The same purified antibody was tested against C-terminal
1113 peptides in the unphosphorylated and phosphorylated forms from H2A.W.6, H2A.W.7, and
1114 H2A.W.12 as above. Note that the H2A.W.7 but not the H2A.W.12 peptide cross reacts with
1115 the H2A.W.6p antibody, indicating that the epitope recognized includes the C-terminal alanine
1116 that is absent in H2A.W.12.

1117

1118

1119

1120

1121

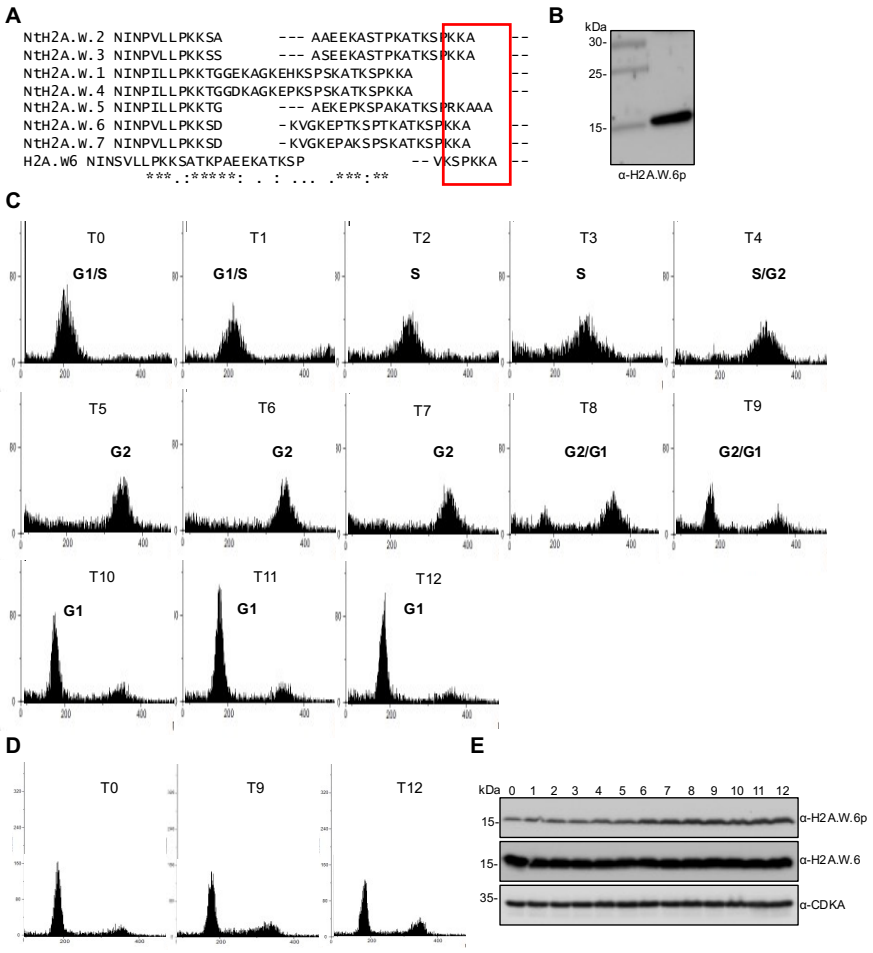

S3 Fig. Phosphorylation of the KSPKK motif changes during the cell cycle. (**A**) Protein sequence alignment of tobacco H2A.W isoforms with *Arabidopsis* H2A.W.6. Only the C-terminal tail is shown, with the conserved KSPKKA motif indicated in a red box. (**B**) Protein extracts from BY-2 cell suspension culture were analysed by western blotting with the anti-H2A.W.6p antibody. Colorimetric and chemiluminescence images were overlaid using the ChemiDoc software to align the position of the signal with the protein ladder. (**C**) Flow cytometry profiles of tobacco BY-2 cell after aphidicolin block and release. Cells were analysed in a time course as in Figure 3A. BY-2 suspension culture was blocked with 20 µg/ml aphidicolin for 24 hours. Upon removal of the aphidicolin block, cells proceeded through the cell cycle in a synchronized manner that was followed by flow cytometry during a twelve-hour time course. (**D**) Control BY-2 cell suspension culture treated with 1% DMSO for 24 hours and then followed over a twelve-hour time course by flow cytometry. Only profiles for time points T0, T9, and T12 are shown. (**E**) Protein extracts from DMSO treated BY-2 cells were analyzed by western blotting with the indicated antibodies. Note that there is no fluctuation of phosphorylated H2A.W.6 (top panel) in unsynchronized cells compared to those synchronized by aphidicolin (see Figure 3A).

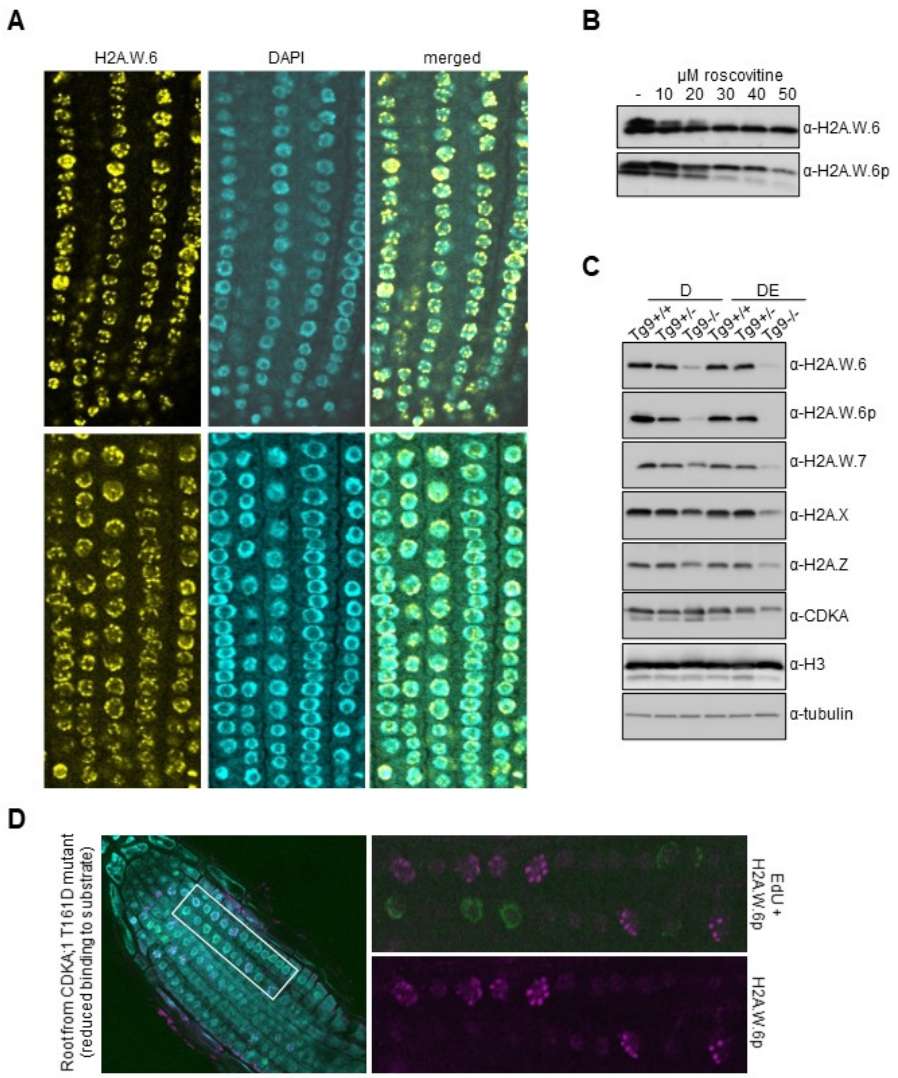

S4 Fig. Phosphorylation of the H2A.W.6 KSPKK motif and expression of H2A.W.6 are linked to CDK activity in *Arabidopsis*. (**A**) Root tips of WT plants were immunostained with the H2A.W.6 antibody. Note that all nuclei display H2A.W.6 signal. Single confocal sections of two root tips are shown. (**B**) One-week old *Arabidopsis* cell suspension culture was treated for 24 hours with the indicated concentrations of roscovitine, a potent inhibitor of cell cycle-dependent kinases. Protein extracts were analyzed by western blotting with H2A.W.6 and H2A.W.6p specific antibodies. (**C**) Transgenic plants expressing weak hypomorphic mutants of CDKA;1, named D and DE, in the *cdka;1* mutant background [51, 52], were genotyped to identify heterozygous and homozygous plants (Tg9+/- and Tg9-/-). Nuclear protein extracts from 2-weeks old seedlings were analyzed by western blotting with the indicated antibodies. (**D**) CDKB;1, which is active at the G2/M transition, also phosphorylates the KSPKK motif of H2A.W.6. Root tips of plants expressing the CDKA;1 T161A hypomorphic mutant that results in reduced substrate binding were immunostained with the H2A.W.6p antibody (magenta) after EdU incorporation (green). Enlarged images on the right demonstrate the presence of H2A.W.6p in G2 nuclei but not in S phase nuclei labeled with EdU. A single confocal section is shown.

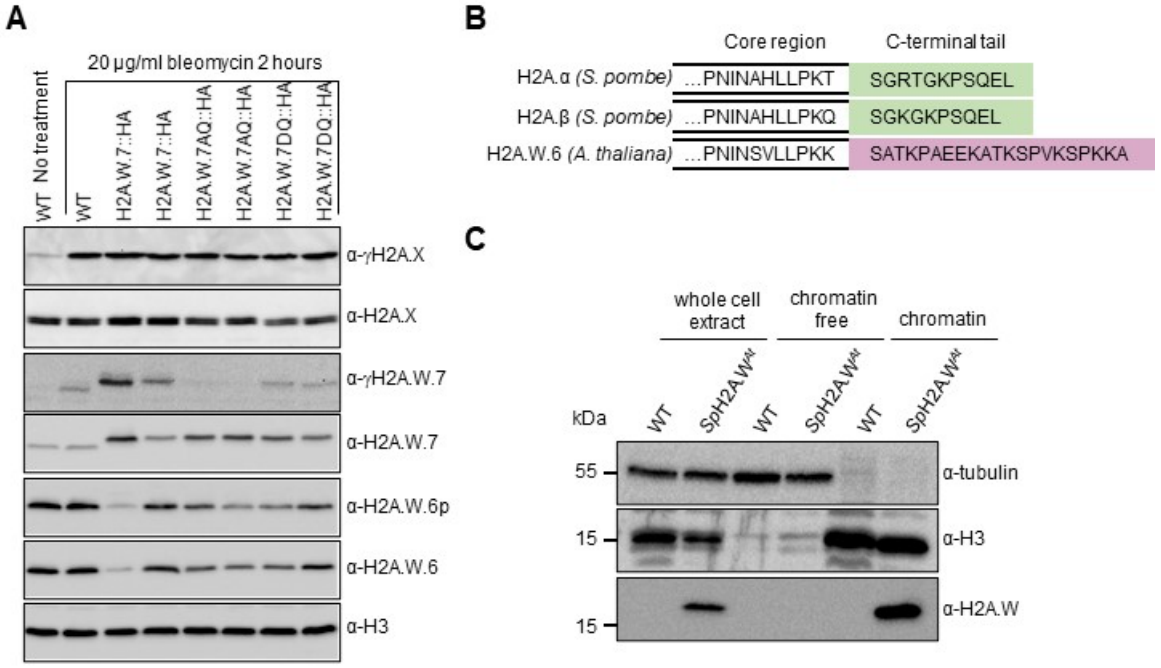

D

Mass spectrometry analysis of fission yeast histone phosphorylation.					
Peptide	*Sp*H2A	*Sp*H2A.W^{At}	*Sp*H2A.W4A^{At}	*Sp*H2ACT	*Sp*H2ACT-AA
TGKPSQEL	1,07E+08				
GKPSQELSATKPAEEK		7,13E+07			
ATKSPVKSPK		3,33E+08			
TSGRTGKPSQELSATKPAEEK			2,62E+07		
LSGRTGKPSQEL				1,09E+08	
TGKPSQELSGR					1,44E+07

S5 Fig. Analysis of KSPKK phosphorylation *in planta* and in *S. pombe*. (**A**) Analysis of γH2A.X, γH2A.W.7, and H2A.W.6p in transgenic seedlings expressing H2A.W.7 hypomorphic mutants in the SQ motif [16] after treatment with 20 µg/ml of bleomycin for 2 hours. Note that bleomycin treatment does not induce phosphorylation of the KSPKK motif on either WT H2A.W.7 or the AQ and DQ mutants of H2A.W.7; this band would be shifted above endogenous H2A.W.6p due to the presence of the HA tag. (**B**) Schematic diagrams of two *S. pombe* H2A variants and *Arabidopsis* H2A.W.6 with the indicated C-terminal tail sequences used for creation of the mosaic H2A variants depicted in Figure 4A. (**C**) Analysis of *Sp*H2A.W^{At} association with the chromatin. Whole cell, chromatin free, and chromatin bound fractions from *Sp*H2A and *Sp*H2A.W^{At} strains were analyzed by western blotting with the indicated antibodies. Tubulin and histone H3 were used as cytoplasmic and nuclear controls, respectively. (**D**) MS analysis of *Sp*H2A SQ motif phosphorylation in fission yeast strains expressing the indicated mosaic or mutated H2A variants. Highly similar levels, quantified as peak areas, of peptides covering phosphorylated SQ motif were measured in all strains.

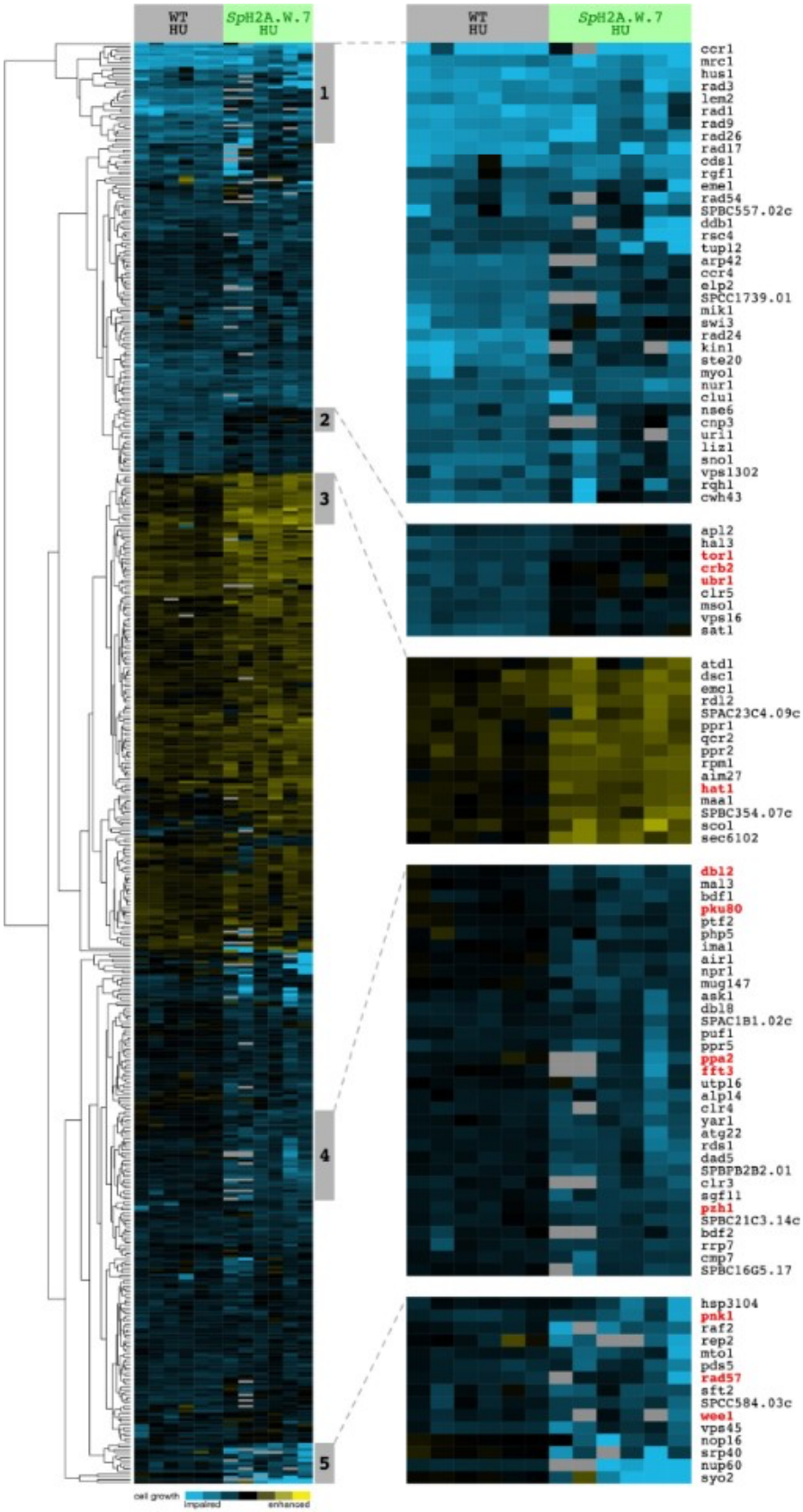

S6 Fig. Cluster analysis of the SGA screen for deletion mutant that suppress growth of spH2A.WAt in 8mM HU plates.